Analysis of Diffusion Limitation in the Alkylation of Benzene over H-ZSM-5 by Combining Quantum Chemical Calculations, Molecular Simulations, and a Continuum Approach

N. Hansen,*,† R. Krishna,‡ J. M. van Baten,‡ A. T. Bell,*,§ and F. J. Keil†

Department of Chemical Engineering, Hamburg University of Technology, D-21073 Hamburg, Germany, Van't Hoff Institute for Molecular Sciences, University of Amsterdam, 1018 WV Amsterdam, The Netherlands, and Department of Chemical Engineering, University of California, Berkeley, CA; 94720-1462

Received: August 15, 2008; Revised Manuscript Received: October 13, 2008

A continuum model based on the Maxwell−Stefan (M-S) equations in combination with the ideal adsorbed solution theory has been used to analyze the influence of adsorption thermodynamics and intraparticle diffusional transport on the overall kinetics of benzene alkylation with ethene over H-ZSM-5. The parameters appearing in the M-S equations were obtained from molecular dynamics simulations, and pure component adsorption isotherms were obtained from configurational-bias Monte Carlo simulations in the grand canonical ensemble. Rate coefficients for the elementary steps of the alkylation were taken from quantum chemical calculations. The intrinsic kinetics of two different reaction schemes were analyzed. The simulations show that all apparent rate parameters of the alkylation are strongly dependent on the reaction conditions. By taking diffusional limitation into account, experimentally determined reaction rates and the orders in the partial pressures of reactants can be reproduced. The results of this study show that empirical power law rate expressions become inappropriate when used to correlate kinetic data over a broad range of conditions. In addition, it is demonstrated that the usual approaches to determine effectiveness factors for reactions in porous media, which assume a constant effective diffusivity, may lead to substantial deviations from rigorous simulations, whereas the simulation model developed here can be used to predict the effectiveness factor for zeolite particles for any set of reaction conditions.

1. Introduction

Gas phase alkylation of benzene using MFI zeolites has been practiced industrially for over two decades.[1–3] Renewed interest in this process has arisen recently due to two developments. The first is the discovery of new synthesis routes for producing zeolites with controlled mesoporosity, which exhibit higher catalytic activity, and sometimes improved selectivity, for reactions such as the alkylation of benzene with ethene.[4,5] The second motivating factor is the possibility of replacing ethene with ethane as the alkylating agent by employing a bifunctional catalyst containing both dehydrogenation and acid sites, for example, PtH-MFI.[6,7] Because intracrystalline diffusion can affect both modes of alkylation, there is considerable interest in developing theoretical methods that could account for the effects of zeolite architecture and particle size, as well as the effects of reactant and product partial pressures and reaction temperature.

Two approaches can be envisioned for describing the diffusion and reaction in zeolites. The first is kinetic Monte Carlo (kMC), a simulation methodology that includes the zeolite pore topology by coarse graining the zeolite lattice in terms of discrete adsorption/reaction sites. In this approach reactant and product molecules are assumed to move between lattice sites by hopping. Transformation of reactants to products can occur at those lattice sites that contain catalytically active centers.[8–13] To make kMC simulations predictive, a large amount of microscopic information has to be determined beforehand in order to generate the list of all single-event probabilities.

The second approach is to use a continuum model with parameter inputs from molecular dynamics for the combined multicomponent diffusion-reaction problem. This approach eliminates the need to provide a list of all single event probabilities but this occurs at the risk of oversimplifying the underlying physical processes. Special care has to be taken to properly describe multicomponent diffusion combined with reaction kinetics, both of which are strongly dependent on the zeolite pore topology and on the molecular loadings within the catalyst. The Maxwell−Stefan (M-S) equations[14,15] have been demonstrated to describe correctly multicomponent diffusion in all-silica zeolites using as data input (a) the single-component diffusivities at zero loading and (b) information on the pure component adsorption isotherms.[14,16–18] Specific guest molecule-zeolite host interactions as well as the lattice topology are included implicitly in the M-S diffusivities, and these parameters can be determined directly from pure component MD simulations for the zeolite of interest. It should be noted that for the M-S equations to be applicable to zeolites with Al/Si > 0, the effect of lattice heterogeneities must be small.[19,20] Low Al/Si ratios (<0.015) are used for the alkylation of benzene in H-ZSM-5,[4] and consequently, the M-S equations are expected to give a reasonable description of the multicomponent diffusion behavior for the constituent species.

The influence of intraparticle diffusional mass transfer on the overall rate of reaction occurring in a catalyst particle is usually characterized by the Thiele modulus, introduced in the late 1930s,[21] and the effectiveness factor derived from it. It is noted, however, that the first solution to the basic mathematical problem underlying the continuum description of the reaction-diffusion problem was presented by Jüttner in 1909.[22] In most analyses of such diffusion-reaction problems the species fluxes are described by Fick's law and the rate of reaction by Langmuir−Hinshelwood or power-law kinetics. Krishna and co-

* To whom correspondence should be addressed. E-mail: n.hansen@tu-harburg.de (N.H.); bell@cchem.berkeley.edu (A.T.B.).
† Hamburg University of Technology.
‡ University of Amsterdam.
§ University of California, Berkeley.

10.1021/jp8073046 CCC: $40.75
Published on Web 12/10/2008

workers[23] have recently demonstrated that for reactions occurring in zeolites Fick's law is only valid for low loadings of weakly confined guest molecules and vanishing correlation effects. When these limiting conditions are not met the correct description of diffusional flux can only be achieved using the M-S equations. Krishna and co-workers[24,25] have also shown that the widely employed multicomponent Langmuir (MCL) approach used to calculate the fractional occupancies of the individual species fails for mixtures containing molecules with different saturation capacities. However, an accurate description of multicomponent adsorption can be obtained using a more sophisticated theory such as the ideal adsorbed solution theory (IAST).[26] Applications of the above concepts to diffusion-reaction problems in zeolites have been reported in refs 23, 24, and 27. For the above-mentioned reasons it is unlikely that the effectiveness factors determined on the basis of the usual approaches used to describe diffusion and reaction in porous media will lead to an accurate description of what actually occurs.

In the present study we show that the M-S equations in combination with IAST can be used to describe the alkylation of benzene with ethene catalyzed by H-ZSM-5. To make these simulations predictive, as many of the parameters as possible were determined from molecular simulations and quantum chemical calculations. A continuum model was used to describe the intrinsic rate of reaction as a function of the local concentration of reactants at the active sites. The results of this work demonstrate that the apparent rate coefficient and the orders in the partial pressures of reactants are not constant but, in fact, are complex functions of the zeolite architecture and particle size and the manner by which the adsorption and diffusion of reacting species influence each other. It is also shown that the simulation model adopted can be used to predict the effectiveness factor for zeolite particles as a function of their size for any set of reaction conditions.

This paper is organized as follows. Section 2 presents the continuum approach used to describe alkylation of benzene with ethene in H-ZSM-5. The methods used to determine the parameters involved in describing adsorption, diffusion, and reactions of all species are presented in Section 3. Predictions determined from the continuum model are compared in Section 4 to predictions from an empirical rate law based on experimental data. The conclusions of this work are presented in Section 5. Details of the simulation methods used to obtain information on the adsorption and diffusion of all species are given in the Supporting Information.

2. Continuum Approach for Diffusion and Reaction

The change of loading with time of component i in a spherical zeolite crystal due to reaction and diffusion is described by the partial differential equation:[28]

$$\frac{\partial q_i}{\partial t} = -\frac{1}{\rho}\frac{1}{\xi^2}\frac{\partial}{\partial \xi}(\xi^2 N_i) + \frac{1}{\rho}\nu_i r; \quad i = 1, 2, ..., n \qquad (1)$$

In this equation, q_i is the loading of species i, ρ is the zeolite density, ξ is the diffusion path, N_i is the molar flux of species i, ν_i is the stoichiometric coefficient, and r is the rate of reaction. We can rewrite eq 1 in terms of the fractional occupancies $\theta_i = q_i/q_{i,\mathrm{sat}}$, which leads to

$$\frac{\partial \theta_i}{\partial t} = -\frac{1}{\rho q_{i,\mathrm{sat}}}\frac{1}{\xi^2}\frac{\partial}{\partial \xi}(\xi^2 N_i) + \frac{1}{\rho q_{i,\mathrm{sat}}}\nu_i r; \quad i = 1, 2, ..., n \qquad (2)$$

The flux of species i, N_i, is calculated using the M-S theory of diffusion. For n-component diffusion, the M-S equations can be written as[29]

$$-\rho\frac{\theta_i}{RT}\nabla\mu_i = \sum_{\substack{j=1 \\ j\neq i}}^{n}\frac{q_j N_i - q_i N_j}{q_{i,\mathrm{sat}} q_{j,\mathrm{sat}} Đ_{ij}} + \frac{N_i}{q_{i,\mathrm{sat}} Đ_i}; \quad i = 1, 2, ..., n \qquad (3)$$

In the latter equation, μ_i is the molar chemical potential of species i, R is the gas constant, T is the absolute temperature, $Đ_i$ is the M-S diffusivity of component i, and $Đ_{ij}$ is the exchange coefficient between species i and j. The exchange coefficient $Đ_{ij}$ quantifies correlation effects. The M-S diffusivity $Đ_i$ is sometimes referred to as the corrected diffusivity. The term on the left-hand side of eq 3 can be expressed in terms of a matrix of thermodynamic correction factors, Γ_{ij}, and the gradient in q_i,

$$\frac{q_i}{RT}\nabla\mu_i = \sum_{j=1}^{n}\Gamma_{ij}\nabla q_j; \quad \Gamma_{ij} \equiv \frac{q_i}{q_j}\frac{\partial \ln f_i}{\partial \ln q_j} = \frac{q_i}{f_i}\frac{\partial f_i}{\partial q_j}; \quad i, j = 1, ..., n \qquad (4)$$

where f_i denote the partial fugacity of species i. Application of eq 4 allows eq 3 to be rewritten in matrix form as

$$(N) = -\rho[\Delta][\Gamma]\nabla(q) \qquad (5)$$

The elements of the matrix $[\Delta]$ can be related to the M-S diffusivities $Đ_i$ and $Đ_{ij}$ by

$$[\Delta] = [B]^{-1} \qquad (6)$$

where the elements of $[B]$ are

$$B_{ii} = \frac{1}{Đ_i} + \sum_{\substack{j=1 \\ j\neq i}}^{n}\frac{\theta_j}{Đ_{ij}}; \quad B_{ij} = -\frac{q_{i,\mathrm{sat}}}{q_{j,\mathrm{sat}}}\frac{\theta_i}{Đ_{ij}}; \quad i, j = 1, 2, ..., n \qquad (7)$$

From eq 3, it is possible to predict the flux of species i, N_i, in a binary (or multicomponent) mixture from pure component diffusion data by making the following two assumptions. First, we assume that $Đ_i$ in the mixture is the same as that for the pure component i estimated at the same occupancy as that of the *total* mixture defined by

$$\theta = \sum_{i=1}^{n}\frac{q_i}{q_{i,\mathrm{sat}}} = \sum_{i=1}^{n}\theta_i \qquad (8)$$

This procedure has been explained in refs 14 and 30. Second, the elements $Đ_{ij}$ are estimated using the interpolation formula presented in refs 18 and 31:

$$q_{j,\mathrm{sat}} Đ_{ij} = [q_{j,\mathrm{sat}} Đ_{ii}]^{q_i/(q_i+q_j)}[q_{i,\mathrm{sat}} Đ_{jj}]^{q_j/(q_i+q_j)} = q_{i,\mathrm{sat}} Đ_{ji} \qquad (9)$$

The self-exchange coefficients $Đ_{ii}$ and $Đ_{jj}$ quantify the correlation effects of pure components i and j; these terms can be determined from the self-diffusivity ($D_{i,\mathrm{self}}$) and the M-S diffusivity for each pure component ($Đ_i$)[29]

$$Đ_{ii} = \frac{\theta_i}{\dfrac{1}{D_{i,\mathrm{self}}} - \dfrac{1}{Đ_i}} \text{ (pure component)} \qquad (10)$$

The self-exchange coefficients can be related to the M-S diffusivity by an empirical correlation[29]

$$\frac{Đ_{ii}}{Đ_i} = a_1 \exp(-a_2\theta_i) + a_3 \exp(-a_4\theta_i) \qquad (11)$$

The constants a_i are obtained from MD simulations of the self- and M-S diffusivities for each of the components in the mixture. It should be emphasized that eq 11 is defined for the pure component i. In the case of mixtures, the fractional

occupancy θ_i has to be replaced by the total occupancy of the mixture, θ (eq 8). M-S diffusivities are almost invariably loading dependent. For molecules whose adsorption isotherms exhibit inflection behavior, that is, can be described by a multisite Langmuir model

$$q = \frac{q_{\text{sat,A}} b_A f}{1 + b_A f} + \frac{q_{\text{sat,B}} b_B f}{1 + b_B f} + ... \tag{12}$$

where $q_{\text{sat,X}}$ denotes the saturation capacity on site X, b_X is the affinity constant, and f is the gas phase fugacity, the following expression for the loading dependence of $Đ$ has been suggested[32]

$$Đ = Đ_A(0)x_A(1 - q_A/q_{\text{sat,A}}) + Đ_B(0)x_B(1 - q_B/q_{\text{sat,B}}) + ... \tag{13}$$

where

$$x_A = \frac{q_A}{\sum_i q_i}, \quad x_B = \frac{q_B}{\sum_i q_i} \tag{14}$$

are the fractions of the total loading present in sites A and B. For benzene and ethylbenzene, there is both theoretical and experimental evidence that these molecules are exclusively located inside the channel intersections below loadings of four molecules per unit cell.[33–38] It is therefore reasonable to assume a linear decrease of $Đ$ with occupancy in this loading regime, that is, $x_B = 0$ in eq 13. This behavior has been proven to occur for 2-methylhexane in MFI by kMC simulations[39] and for *iso*-butane by both kMC and experimental studies.[40]

The loading dependency of the ethene diffusivity can be approximated by the simple relation

$$Đ = Đ(0)(1 - \theta) \tag{15}$$

In the present study we used the model of Reed and Ehrlich,[41] giving an improved description

$$Đ = Đ(0)\frac{(1 + \varepsilon)^{z-1}}{(1 + \varepsilon/f)^z} \tag{16}$$

with

$$\varepsilon = \frac{(\beta - 1 + 2\theta)f}{2(1 - \theta)}; \quad \beta = \sqrt{1 - 4\theta(1 - \theta)(1 - 1/f)};$$
$$f = a \exp(b\theta) \tag{17}$$

The parameter z is the coordination number representing the maximum number of nearest neighbors. The factor f accounts for interaction between neighboring molecules. The parameters a and b are obtained by fitting them to MD data (see Krishna et al.[29] for more detailed discussions and derivations).

We have shown previously[42] that the mechanism of benzene alkylation can be represented by a one-step mechanism involving the following elementary processes:

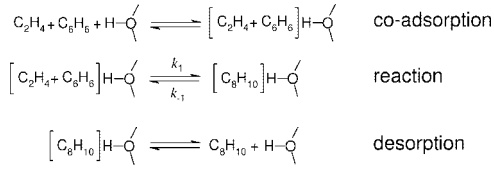

The rate equation corresponding to this mechanism is:

$$\frac{r}{\rho} = \tilde{r} = k_1 q_{\text{E+B,H+}} - k_{-1} q_{\text{EB,H+}} \tag{18}$$

where k_1 and k_{-1} are the rate coefficients for the forward and reverse reaction of ethene and benzene to form ethylbenzene, respectively; $q_{\text{E+B,H+}}$ is the amount of coadsorbed "ethene + benzene" at the active sites and $q_{\text{EB,H+}}$ is the amount of adsorbed ethylbenzene at the active sites. The application of eq 18 within the continuum approach requires analytical expressions to calculate $q_{\text{E+B,H+}}$ and $q_{\text{EB,H+}}$ from the species loadings q_E, q_B, and q_{EB}. For the derivation of such expressions it is assumed that benzene and ethylbenzene are located exclusively inside the channel intersections below loadings of four molecules per unit cell (see above). Furthermore, it is assumed that the acid sites are also located exclusively inside the intersections between the straight and the sinusoidal channel or, more precisely, on the O atom next to the T12 site at the aperture of the sinusoidal channel (see ref 42 for details). In fact, the location of the ethene molecule in the coadsorbed state can be characterized as in between the intersection and the sinusoidal channel. The third assumption is the equal accessibility of all adsorption sites for ethene. The maximum adsorption capacity of $q_{\text{E,sat}} = 22$ molecules per unit cell was obtained from MC simulations. This number is set equal to the number of adsorption sites available for ethene. These 22 sites are distributed over four intersections, four sinusoidal channels, and four straight channels out of which the intersections have the largest free volume. Monte Carlo simulations carried out with all intersections artificially blocked with benzene molecules give a maximum ethene adsorption capacity of about nine molecules per unit cell, that is, each adsorbed benzene reduces the number of sites available for ethene adsorption by 3.25 molecules per unit cell. Likewise, MC simulations with all intersections artificially blocked by ethylbenzene have shown that each adsorbed ethylbenzene reduces the number of sites available for ethene by around 3.5 molecules per unit cell. Finally, we assume that if benzene occupies an intersection, the probability of ethene adsorption next to this benzene (defined as coadsorption) is the same as that of ethene adsorption at any other free site within the unit cell. For the number of adsorption sites per unit cell accessible for ethene in a ternary mixture of ethene, benzene, and ethylbenzene, $q_{\text{E,tot}}$, we can then write

$$q_{\text{E,tot}} = 22 - 3.25q_B - 3.5q_{EB} \tag{19}$$

where q_B is the number of benzene molecules per unit cell and q_{EB} is the number of ethylbenzene molecules per unit cell. Next, we need to know, how many of the $q_{\text{E,tot}}$ sites are potentially available for coadsorption of benzene and ethene. This number is dictated by the number of benzene molecules present, such that the fraction of ethene coadsorbed with benzene is $q_B/q_{\text{E,tot}}$ and the concentration of coadsorbed "ethene + benzene", $q_{\text{E+B}}$, can be obtained from

$$q_{\text{E+B}} = \frac{q_B}{22 - 3.25q_B - 3.5q_{EB}} q_E \tag{20}$$

To complete the model for the forward rate we need to take into account that not every intersection contains a proton. Therefore, we introduce γ as the number of protons per unit cell which are located in an intersection and define

$$\lambda = \frac{\gamma}{4} \tag{21}$$

as the active site density (average number of acid sites per intersection). In addition, we need to note that each ethylbenzene

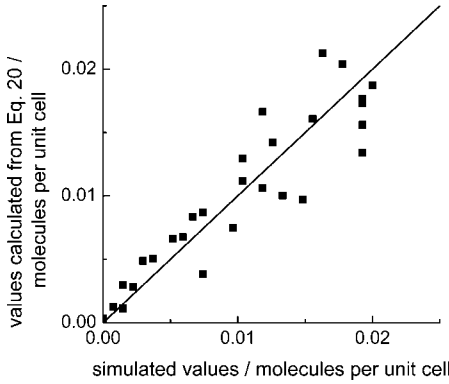

Figure 1. Amount of coadsorbed ethene plus benzene in the channel intersections of MFI at 653 K and various compositions of the corresponding ternary gas phase mixture as predicted by eq 20 and Monte Carlo simulations using a sampling radius of 4.8 Å. The total pressure was varied between 1×10^5 and 11×10^5 Pa.

molecule present in the unit cell occupies an intersection that, if it were active, cannot be used for the forward reaction. Therefore, the active site density has to be lowered by the factor

$$\frac{q_B}{q_B + q_{EB}} \tag{22}$$

In summary, the concentration of coadsorbed "ethene + benzene" at an acid site containing intersection becomes

$$q_{E+B,H+} = \frac{q_B}{22 - 3.25q_B - 3.5q_{EB}} \cdot q_E \cdot \frac{q_B}{q_B + q_{EB}}\lambda \tag{23}$$

A similar derivation can be used for the amount of adsorbed ethylbenzene at an acid site containing intersection. For $q_{EB,H+}$ we can write

$$q_{EB,H+} = q_{EB}\frac{q_{EB}}{q_B + q_{EB}}\lambda \tag{24}$$

The validity of eq 20 was tested against MC simulations for different ethene−benzene−ethylbenzene mixtures. After every few cycles the configuration inside the pore was stored. These configurations were then been analyzed to determine the numbers of coadsorbed "ethene + benzene" molecules. A configuration was interpreted as coadsorbed if an ethene molecule was located next to an intersection occupied by benzene such that one of the distances between the carbon atoms of ethene and the center of the intersection was smaller than the specified sample radius. This method of counting is based on the active site model used in our DFT study[42] where the acid site is assumed to be located on the O atom next to the T12 site at the aperture of the sinusoidal channel (see above). The sample radius was determined by the condition that for a unit cell in which all intersections are occupied by benzene while the remaining pore space is completely filled with ethene, the number of coadsorbed configurations should be four molecules per unit cell. This condition was fulfilled for a sampling radius of 4.8 Å. As can be seen in Figure 1, the concentration of coadsorbed "ethene + benzene" obtained from MC simulations agrees reasonably well with the concentration estimated by means of eq 20. It can therefore be concluded that eq 20 is sufficiently accurate to be used for an estimation of the coadsorbed amount of "ethene + benzene" in the continuum model.

We have also shown previously[42] that the alkylation of benzene by ethene can be described by a two-step mechanism involving the following elementary processes:

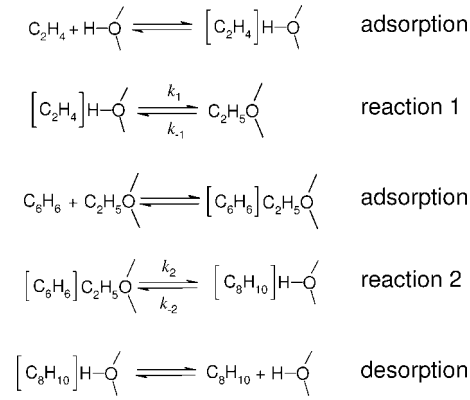

Expressions analogous to eqs 23 and 24 can be derived for the two-step mechanism of benzene alkylation with ethene (see Appendix D of the Supporting Information). These are given by

$$q_{E,H+} = \frac{13 - 3.25(q_B + q_{EB} + q_{eth})}{22 - 3.25q_B - 3.5q_{EB} - q_{eth}}q_E\lambda \tag{25}$$

and

$$q_{eth+B} = \frac{q_B}{4 - q_{EB}}q_{eth} \tag{26}$$

for the amount of ethene adsorbed at the Brønsted acid sites, $q_{E,H+}$, and the amount of benzene adsorbed next to an ethoxide, q_{eth+B}.

The system of partial differential equations (eq 2) was discretized with respect to the spatial coordinate using central differences (method of lines), and the resulting system of ordinary differential equations was integrated using a fourth order Runge−Kutta scheme until the solution was stationary (see Appendix E of the Supporting Information for details). The profile of species concentration, $q(\xi)$, was taken to be symmetric at the center of the crystal, whereas the concentration of each species at the crystal surface was fixed to the value determined by adsorption equilibrium. Determination of the thermodynamic factors (eq 4) requires the calculation of the derivative of the partial fugacities with respect to the species concentrations. Details of these computations are given in ref 43. Species fugacities inside the zeolite were calculated as partial fugacities of a hypothetical gas phase corresponding to the actual loading within the zeolite and were obtained by means of the IAST in its inverse formulation.[26,44]

3. Parameterization

Pure component adsorption isotherms were obtained by MC simulation using the method described in Appendix A of the Supporting Information. These isotherms were fitted to a three-site Langmuir model (see Appendix B of the Supporting Information). Mixture adsorption isotherms were then calculated from the pure component adsorption isotherms by means of the IAST.[26] As shown in Appendix B of the Supporting Information, IAST provides an accurate description of the adsorption isotherms for mixtures in the pressure regime relevant for the alkylation of benzene with ethene. The rate coefficients for the alkylation of benzene with ethene and the reverse reaction were determined in two steps.[42] The intrinsic activation energies of these processes were calculated by applying single-point MP2-corrections to DFT-converged stationary states on a large cluster model. This approach was justified using smaller clusters by

TABLE 1: Intrinsic Rate Constants for the One-Step and Two-Step Mechanisms

		T (K)					
		calcd values[42]			readjusted (effective) values (this work)		
reaction scheme	constant	603	653	703	603	653	703
one-step	k_1, s^{-1}	8.17×10^{-1}	4.97×10^{0}	2.33×10^{1}	1.14×10^{2}	6.96×10^{2}	3.27×10^{3}
	k_{-1}, s^{-1}	3.80×10^{-5}	9.75×10^{-4}	1.58×10^{-2}	5.32×10^{-3}	1.37×10^{-1}	2.21×10^{0}
two-step	k_1, s^{-1}	2.58×10^{2}	1.14×10^{3}	4.11×10^{3}			
	k_{-1}, s^{-1}	1.20×10^{1}	1.12×10^{2}	7.65×10^{2}			
	k_2, s^{-1}	3.19×10^{2}	1.84×10^{3}	8.26×10^{3}			
	k_{-2}, s^{-1}	7.24×10^{-1}	6.98×10^{0}	4.87×10^{1}			

comparing intrinsic activation energies obtained from MP2-optimized structures to those obtained from single point MP2-calculations on DFT-converged structures. The energy difference was <0.2 kcal/mol. Preexponential factors were determined using transition state theory (TST). For a detailed discussion of the level of theory used for obtaining the rate parameters as well as of the size of the model system used the reader is referred to the theory section of ref 42. The rate coefficients obtained by this means are presented in Table 1. The rate coefficients for the one-step scheme are 2.5 orders of magnitude smaller than those for the two-step scheme. While this could lead to the conclusion that the one-step scheme is irrelevant, it should be kept in mind that the rate coefficient for ethoxide formation (the first step in the two-step scheme) was calculated assuming that ethene enters an empty intersection. An excess of benzene is used in industrial practice. This lowers the probability that ethene finds an unoccupied intersection, since benzene adsorbs much more strongly than ethene in the channel intersections. It is therefore likely that both mechanisms take place simultaneously. Thus, the extent to which each mechanism contributes to the overall activity is hard to establish. As a consequence, the overall kinetics of benzene alkylation were examined for both mechanisms and compared with experimental data of Christensen et al.[4]

The intrinsic activation barrier for the one-step alkylation of benzene with ethene determined from QM calculations is $E^{\ddagger} = 120.5$ kJ mol^{-1} and the intrinsic pre-exponential factor at 653 K is $A = 2.5 \times 10^{10}$ s^{-1}.[42] For the two-step scheme the intrinsic activation barriers determined from QM calculations are $E_1^{\ddagger} = 99.2$ kJ mol^{-1} and $E_2^{\ddagger} = 110.5$ kJ mol^{-1}, and the intrinsic pre-exponential factors at 653 K are $A_1 = 1.1 \times 10^{11}$ s^{-1} and $A_2 = 1.4 \times 10^{12}$ s^{-1}, respectively.[42] The values from theory cannot be compared with the apparent activation energy and apparent preexponential factor determined from experimental data, since the values of the apparent activation energy and preexponential factor depend on reaction conditions. To proceed, the rate of reaction per unit mass of catalyst as function of temperature and total pressure was simulated, maintaining the same benzene to ethene ratio in the gas phase (B/E = 5) as was used in the experiments performed by Christensen et al.[4] These authors investigated the alkylation of benzene with ethene over mesoporous H-ZSM-5 synthesized by the carbon templating method.[45] They reported an average distance between the mesopores of 0.04 μm leading to the conclusion that the measured reaction rates were not influenced by intraparticle diffusion.[4,5] The turnover frequency and the apparent activation energy were calculated for a pressure of 2.5×10^5 Pa using the theoretically determined rate coefficients for the one-step scheme.[42] These simulations underestimated the experimentally observed turnover frequency by a factor of around 400 and the apparent activation energy by 15 kJ/mol. By contrast, the simulated values using the theoretically determined rate coefficients for the two-step scheme overestimated the experimentally observed turnover frequency at 2.5×10^5 Pa by a factor of 4 and the apparent activation energy by 5 kJ/mol. As already noted above, the extent to which each mechanism contributes to the overall activity is hard to establish. To proceed we determined *effective* intrinsic rate coefficients by adjusting the theoretically determined ones so that the experimental data were reproduced reasonably well. Due to the smaller number of parameters required, these effective rate coefficients were based on the one-step mechanism. Furthermore, the decision was made to match not only the experimental data of Christensen et al.[4] but also those of Lu et al.[46] (see Section 4.2). Therefore, the rate coefficients presented in the right-hand side of Table 1 represent a compromise between the desire to reproduce the Arrhenius plot of Christensen et al.[4] exactly and the desire to match kinetic data reported by Lu et al.[46] This objective could be achieved by multiplying the theoretically determined pre-exponential factor by a factor of 140, while leaving the theoretically determined intrinsic activation energy unchanged. As seen in Figure 2, good agreement was obtained between the simulated Arrhenius plot and the experimental Arrhenius plot of Christensen et al.,[4] assuming a simulation pressure of 5.0×10^5 Pa (see upper curve of Figure 2). It should be noted that agreement with the experimental data could also be achieved by carrying out the simulation at 2.5×10^5 Pa, but this required adjustment of the activation energy in addition to the preexponential factor. Such adjustement, however, would lead to simulated rates that deviate from the data of Lu et al.[46] In particular, the apparent activation energy determined from

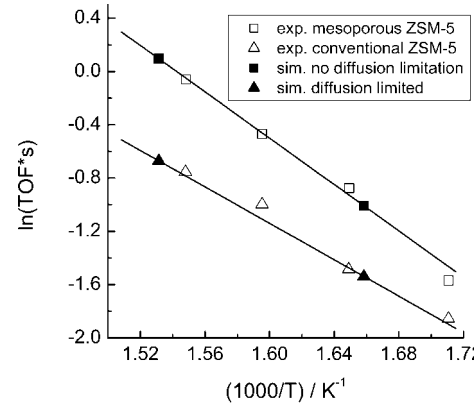

Figure 2. Experimental[4] and simulated Arrhenius plots for the ethylation of benzene. The experimental data are reported for both mesoporous H-ZSM-5 and a sample of H-ZSM-5 free of mesopores at a total pressure of 2.5×10^5 Pa and a benzene to ethene ratio of 5.1. The conditions for the simulation were $p = 5 \times 10^5$ Pa, $y_B = 0.8338$, $y_E = 0.1660$, $y_{EB} = 0.0002$. For simulations of the turnover frequency in the mesoporous sample of H-ZSM-5 the exterior surface loadings were used. For the simulation of the turnover frequencies in the nonmesoporous sample of H-ZSM-5 the zero-loading MD diffusivities were scaled down by 3.4 orders of magnitude (see Table 2). The intrinsic rate constants used are listed on the right-hand side of Table 1.

TABLE 2: Adjusted Zero-Loading M-S Diffusivities for Ethene, Benzene, and Ethylbenzene

molecule	temperature [K]	$Đ_i(0)$ [10^{-13} m^2 s^{-1}]
C_2H_4	603	87.6
C_2H_4	653	99.5
C_2H_4	703	99.5
C_6H_6	603	1.6
C_6H_6	653	2.0
C_6H_6	703	2.8
C_8H_{10}	603	1.3
C_8H_{10}	653	1.6
C_8H_{10}	703	2.2

simulation would now overestimate that determined experimentally by a significant amount (see Section 4.2). Clearly, then a more accurate evaluation of the theoretically determined rate coefficients, requires a larger source of experimental data taken in the absence of intraparticle diffusional limitations over a wide range of temperatures and reactant partial pressure. Nevertheless, the effective rate coefficients obtained by the methods discussed can be used to analyze the effects of intraparticle diffusional mass transport on the alkylation of benzene with ethene occurring in H-ZSM-5.

M-S diffusivities were extracted from extensive MD simulation campaigns as outlined in Appendix C of the Supporting Information. The extracted zero-loading M-S diffusivities, $Đ_i(0)$, for ethene in the temperature range 603−703 K are of the order 10^{-8} m^2 s^{-1}. Experimental diffusivities of ethene at these temperatures are not available in the literature. However, at 300 K the simulated zero loading diffusivity is 0.9×10^{-8} m^2 s^{-1} and thus in reasonable agreement with reported experimental values for ethane and ethene in MFI.[47–50] It should be noted that some authors report considerably smaller values[51,52] that are of the order 10^{-11} m^2 s^{-1} at room temperature. However, these values were most likely influenced by external transport resistances.[51]

For benzene and ethylbenzene, the extracted M-S diffusivities in the temperature range 603−703 K are of the order of 10^{-10} m^2 s^{-1}, which is significantly higher than most of the values reported experimentally. Thus, it becomes necessary to review what is known from both experiments and theory about the diffusivity of benzene and ethylbenzene.

The diffusion of benzene in MFI has been the subject of numerous experimental studies over the last 25 years.[53–77] At room temperature most of the data lie in the range of 1×10^{-15} m^2 s^{-1} (ref 53) to 7×10^{-14} m^2 s^{-1} (ref 55). Diffusion coefficients at higher temperatures have been estimated by extrapolation and are most often above of 10^{-11} m^2 s^{-1} at 600 K.[62] However, direct measurements have been reported to yield smaller diffusivities.[67,77] For example, Masuda et al.[67] report an intracrystalline diffusivity for benzene of 5×10^{-14} m^2 s^{-1} at 650 K. At this high temperature no difference was found between diffusion coefficients in silicalite and H-ZSM-5. At lower temperature, diffusivities in H-ZSM-5 have measured to be lower by 50% than those for silicalite. Measurements of the diffusion coefficient for ethylbenzene in MFI show a variation in the order of magnitude similar to that reported for benzene.[53,59,63,65,71,78]

A number of theoretical efforts have been made to estimate the diffusion coefficient for benzene. Conventional MD simulations are hampered by the long simulation times required for a reliable estimate of the diffusion coefficient. Rungsirisakun et al.[79] have reported a value of $D_{self}(300\ K) \approx 10^{-10}$ m^2 s^{-1}; however, the simulation time used by these authors (100 ps) was probably be too small to give a reliable estimate for the self-diffusion coefficient. Other authors have estimated the self-diffusion coefficient to be on the order of 10^{-15} m^2 s^{-1} to 10^{-12} m^2 s^{-1} based on MD simulations.[80,81] Constrained reaction coordinate dynamics and dynamic MC simulations have also been used to estimate the diffusivity. Values of $D_{self}(300\ K) \approx 10^{-14}$ m^2 s^{-1} have been reported using these methods.[82,83] Takaba et al.[84] obtained a value of $D_{self}(300\ K) \approx 10^{-15}$ m^2 s^{-1} by means of dynamic MC simulations with rate constants estimated from semiempirical quantum chemical calculations, and Snurr et al.[85] obtained values of $D_{self}(300\ K) \approx 10^{-16}$ m^2 s^{-1} from transition state theory calculations.

It is evident from the preceding discussion that reliable values of the zero-loading M-S diffusivities for benzene and ethylbenzene are not known and that the values estimated from MD mixture simulations in the present study are most likely too high. To deal with this problem, we have proceeded in the following way. Christensen et al.[4] have reported an Arrhenius plot for benzene alkylation with ethene by H-ZSM-5 in which the zeolite crystallites had an average size about 2 μm. In this case, a significantly lower activity was observed relative to that seen for mesoporous H-ZSM-5, which the authors ascribed to diffusion limitation. We were able to match these data by simulation if the zero-loading M-S diffusivities for all species were reduced by 3.4 orders of magnitude (see lower curve in Figure 2). For these simulations we used the same rate coefficients as in the absence of diffusion limitation (see above). The resulting diffusivities for ethene are then of the order 10^{-11} m^2 s^{-1}, while those for benzene and ethylbenzene are of the order 10^{-13} m^2 s^{-1} (see Table 2). Whereas the values obtained for benzene and ethylbenzene lie within the range of the experimental data discussed above, the scaled diffusivity for ethene is underestimated by one to 2 orders of magnitude. However, by scaling all diffusivities by the same factor the ratios between the zero-loading diffusivities as well as the coefficients describing loading dependency and self-exchange could be taken directly from the MD results summarized in Tables SC1 and SC2 of the Supporting Information. Moreover, the overall activity of the crystallite is dominated by the diffusivities of benzene and ethylbenzene. The sensitivity of the simulated reaction rates with respect to the zero-loading diffusivity of ethene and the binary exchange parameters is discussed in Section 4.2.

4. Results and Discussion

4.1. Intrinsic Kinetics. The intrinsic kinetics predicted by the model in the absence of diffusional mass transfer limitations can be established by examining plots of $q_{E+B,H+}$ (see eq 23) versus p_E and p_B. Figures 3 and 4 show such plots for 653 and 703 K calculated on the assumption that $q_{EB} \approx 0$ and $\gamma = 4$. It is evident that at both temperatures the predicted dependence of the rate on the ethene partial pressure is essentially 1.0, whereas the dependence on the partial pressure of benzene is 0.4 at 653 K (Figure 3b) and rises to 0.6 at 703 K (Figure 4b). Additional calculations with $p_B = 10 \times 10^5$ Pa and $p_E = 3 \times 10^5$ Pa show that these numbers are essentially unaffected by the partial pressure of the coadsorbed species (see Figure SG1 in the Supporting Information). The change in the dependence on benzene partial pressure with temperature is a reflection of the effects of temperature on the adsorption of benzene from an ethene-benzene mixture. Figure 5shows Arrhenius plots of the turnover frequency of benzene alkylation with ethene versus inverse temperature for a fixed ratio of benzene to ethene and different total pressures, ranging from 1×10^5

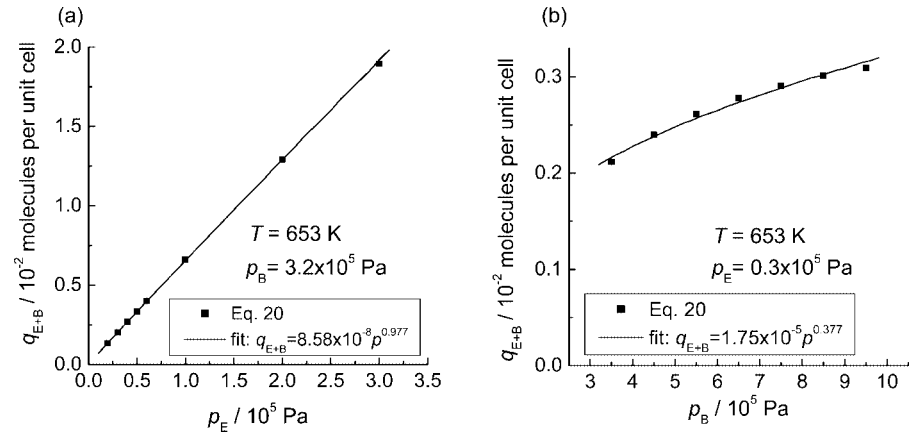

Figure 3. (a) Dependence of the amount of coadsorbed $C_2H_4 + C_6H_6$ on the ethene partial pressure at a fixed benzene partial pressure of 3.2 × 10^5 Pa and a fixed ethylbenzene partial pressure of 35 Pa at 653 K. (b) Dependence of the amount of coadsorbed $C_2H_4 + C_6H_6$ on the benzene partial pressure at a fixed ethene partial pressure of 0.3 × 10^5 Pa and a fixed ethylbenzene partial pressure of 35 Pa at 653 K.

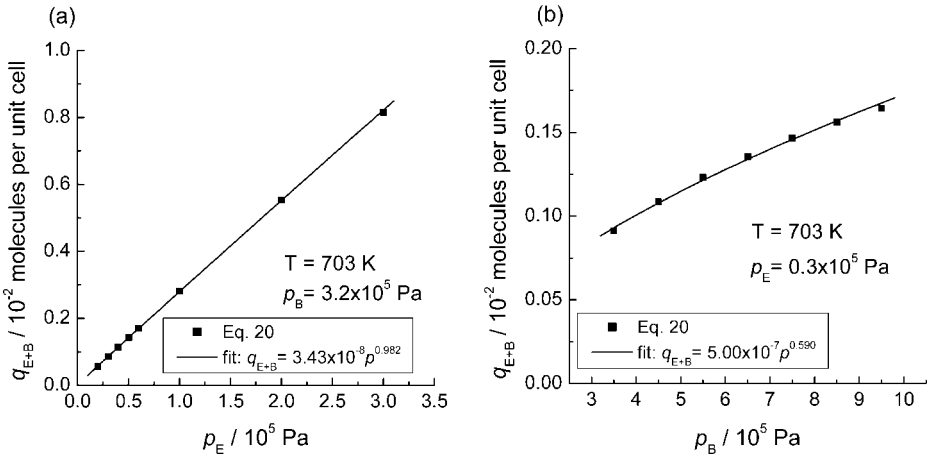

Figure 4. (a) Dependence of the amount of coadsorbed $C_2H_4 + C_6H_6$ on the ethene partial pressure at a fixed benzene partial pressure of 3.2 × 10^5 Pa and a fixed ethylbenzene partial pressure of 35 Pa at 703 K. (b) Dependence of the amount of coadsorbed $C_2H_4 + C_6H_6$ on the benzene partial pressure at a fixed ethene partial pressure of 0.3 × 10^5 Pa and a fixed ethylbenzene partial pressure of 35 Pa at 703 K.

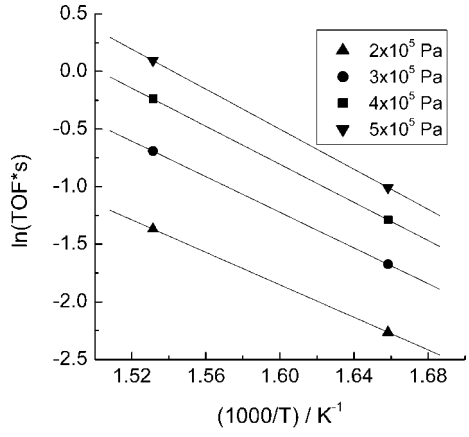

Figure 5. Arrhenius plots illustrating the pressure dependence of the apparent activation energy and the apparent preexponential factor.

to 5 × 10^5 Pa. It is evident that both the apparent activation energy and the apparent preexpontial factor are functions of the total pressure. The corresponding values are listed in Table 3. The changes in these parameters are a direct consequence of the pressure and temperature dependency of the mixture adsorption equilibrium.

The results presented in Figures 3−5 clearly demonstrate that empirical power law kinetics cannot be used to describe

TABLE 3: Apparent Rate Parameters Obtained from Simulations for Different Total Pressures at Constant $p_B/p_E = 5$

p [10^5 Pa]	E_{app} [kJ mol^{-1}]	A_{app} [s^{-1}]
2.0	58.7	1.25 × 10^4
3.0	64.3	6.95 × 10^4
4.0	68.7	2.46 × 10^5
5.0	72.3	6.63 × 10^5

the rate of benzene alkylation with ethene over H-ZSM-5 even in the absence of diffusional mass transfer. While such expressions may be useful for correlating results over a narrow range of reaction conditions, they become increasingly inappropriate as the range of reaction conditions broadens and all of the apparent rate parameters (e.g., pre-exponential factor, activation energy, and reaction order) become functions of the reaction conditions.

4.2. Effects of Diffusional Mass Transfer. Figure 6 illustrates the intraparticle concentration profiles of all species corresponding to the diffusion limited simulation at 653 K along with the turnover frequency as function of the radial coordinate. The figure shows that the benzene to ethene ratio on the exterior surface is higher by a factor of 6 than the ratio of partial pressures in the gas phase due to the differences in adsorption strength. It should be emphasized that the loading of ethylbenzene on the exterior surface is not zero but has a small value of 6.6 × 10^{-4} molecules per unit cell corresponding to a gas phase

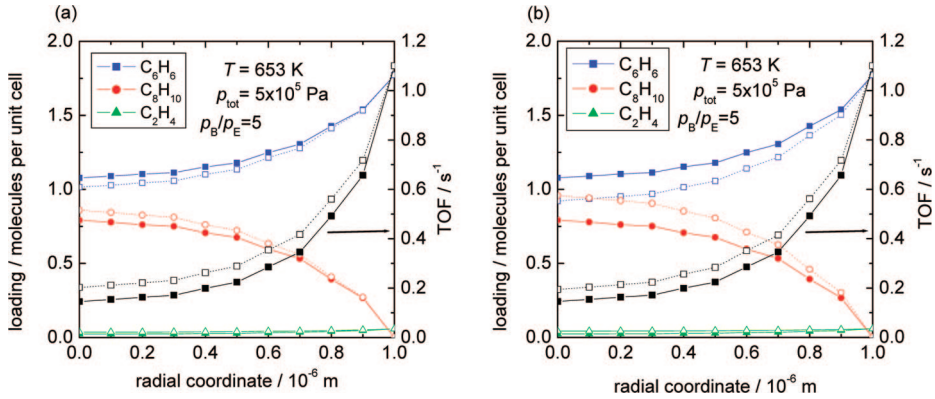

Figure 6. Radial concentration and turnover frequency profiles for different diffusion-limited scenarios. Solid lines represent: finite exchange and scaled diffusivities, that is, zero-loading M-S diffusivities were taken from Table 2, and the parameters describing self-exchange were taken from Tables SC1 and SC2 of the Supporting Information. Dotted lines represent: (a) facile exchange scenario, that is, $Đ_{ij} \rightarrow \infty$ and (b) unscaled ethene zero loading diffusivity, that is, $Đ_E(0) = 2.5 \times 10^{-8}$ m^2 s^{-1}.

pressure of 35 Pa. In practice these conditions would be found at the reactor entrance. Due to diffusion limitations a strong increase of the product concentration toward the particle center takes place, accompanied by a strong decrease of the reactant concentrations.

The concentration profiles shown in Figure 6a were calculated for two exchange scenarios. The full symbols represent the *finite* exchange scenario, that is, the binary exchange coefficients $Đ_{ij}$ were obtained using the logarithmic interpolation formula (eq 9) along with eq 11 for the calculation of the self-exchange coefficients. The open symbols represent the *facile* exchange scenario, that is, the binary exchange coefficients approach infinity, resulting in a diagonal matrix [Δ]. MD mixture simulations clearly show the existence of correlation effects for the present system (see Appendix C in the Supporting Information). It is of interest, however, to assess the significance of the exchange coefficients on the simulated concentration profiles. As seen in Figure 6a, correlation leads to higher reactant and lower product concentrations compared to uncorrelated diffusion. The largest effect of correlation has been calculated for the ethene concentration profile, due to the presence of the slow diffusing species benzene and ethylbenzene. While in the finite exchange scenario the ethene concentration in the particle center has decreased to 39% of its exterior surface value, this concentration drop is less distinct in the facile exchange scenario. In the latter case, the ethene concentration in the particle center has decreased to 61% of its exterior surface value. The effect on the benzene concentration is relatively small. In the finite exchange scenario the concentration at the particle center is 61% of its exterior surface concentration, while in the facile exchange scenario this value is 57%. Because ethene is the limiting species, the overall activity of the catalyst particle is higher by a factor of 1.1 in the facile exchange scenario. The effectiveness factors are 0.47 for the finite exchange scenario and 0.52 for the facile exchange scenario. Thus, we can conclude that while the inclusion of correlation effects in the M-S equations give a physically correct description of multicomponent diffusion, the degree of correlations has a relatively little influence on the calculated effects of diffusive mass transfer for the present system. These effects are dominated by the diffusivities of benzene and ethylbenzene due to their significantly higher loadings within the zeolite compared to ethene.

A further point to be addressed is the effect of reducing the magnitude of ethene diffusivity. Concentration profiles of all species were calculated using the M-S diffusivity for ethene obtained from MD simulations at 653 K, that is, 2.5×10^{-8} m^2 s^{-1}, while keeping the diffusivities for benzene and ethylbenzene at their reduced values (see above). As a result the diffusivity of ethene was five orders of magnitudes larger than those of benzene and ethylbenzene. The calculated concentration profiles are shown in Figure 6b (note that the finite exchange scenario was used for these calculations). The ethene concentration in the particle center increased to 72% of its exterior surface value. The benzene concentration in the particle center has dropped to 52% of its exterior surface value. By contrast, the ethene concentration dropped to 39% for the case of the reduced diffusivity of 9.95×10^{-12} m^2 s^{-1} (see Figure 6a). The profile of the turnover frequency is similar to that for the case of facile exchange as is the value of the effectiveness factor (0.52). Therefore, the influence of the higher ethene diffusivity on the profile of catalytic activity is limited.

Figures 7 and 8 show the dependence of the overall rate of benzene alkylation with ethene predicted for a particle of H-ZSM-5 as functions of p_E and p_B and temperatures of 653 and 703 K. In both cases, the particle is assumed to have a diameter of 2 μm. Also shown on these plots are the rates predicted by the power law expression developed by Lu et al.[46] to describe the alkylation of benzene by ethene on AB-97 (AB-97 refers to a catalyst consisting mainly of H-ZSM-5 and alumina. The simulated rates per unit mass of MFI have been converted to rates per unit mass of AB-97, as outlined in Appendix F of the Supporting Information.) for ethene pressures of 0.3×10^5 to 3×10^5 Pa, benzene pressures of 3×10^5 to 13×10^5 Pa, and temperatures of 653−723 K. For this range of conditions, these authors reported values for n_E and n_B of 0.795 and 0.110, respectively, and a value for n_{EB} of 0.28. These orders and the values of the apparent pre-exponential factor and activation energy are given in Table 4.

It is evident from Table 4 that the activation energy appearing in the empirical rate law (21.7 kJ mol^{-1}) is significantly lower than the values obtained by Christensen et al.[4] and those predicted by our model. Although the physical significance of this number is limited (see above), the deviation from the data of Christensen et al.[4] may suggest the occurrence of external particle mass transfer limitation in addition to intraparticle diffusional limitation. The pellet size used by Christensen et al.[4] was smaller by a factor of 10 than that used by Lu et al.[46] The latter authors also performed measurements using smaller pellet sizes and fitted these results to a Langmuir−Hinshelwood expression. The activation energy obtained in this case was 42.5 kJ mol^{-1}. However, the significance of this value is limited because of the inherently incorrect partial pressure dependences

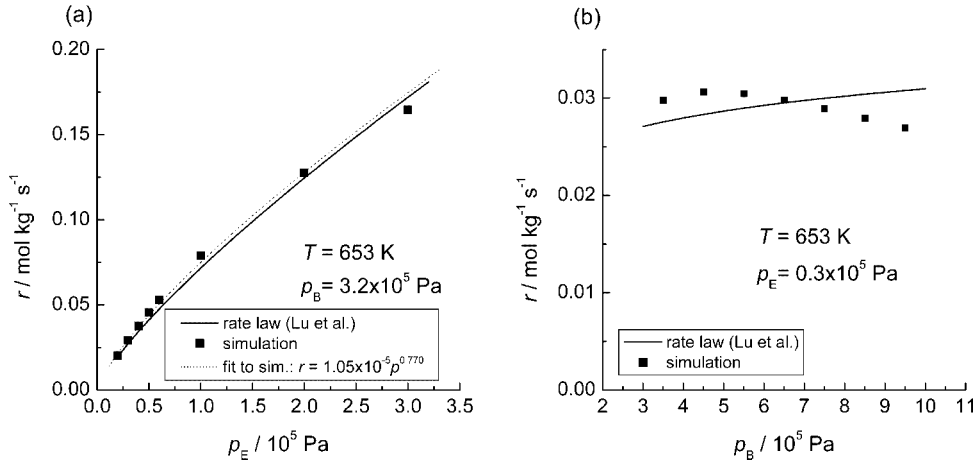

Figure 7. Simulated and experimental rates per unit mass of catalyst for the alkylation of benzene with ethene. (a) Constant benzene partial pressure of 3.2×10^5 Pa at 653 K; (b) constant ethene partial pressure of 0.3×10^5 Pa at 653 K. The partial pressure of ethylbenzene was fixed to 35 Pa. The experimental data were calculated using the rate expression of Lu et al.[46]

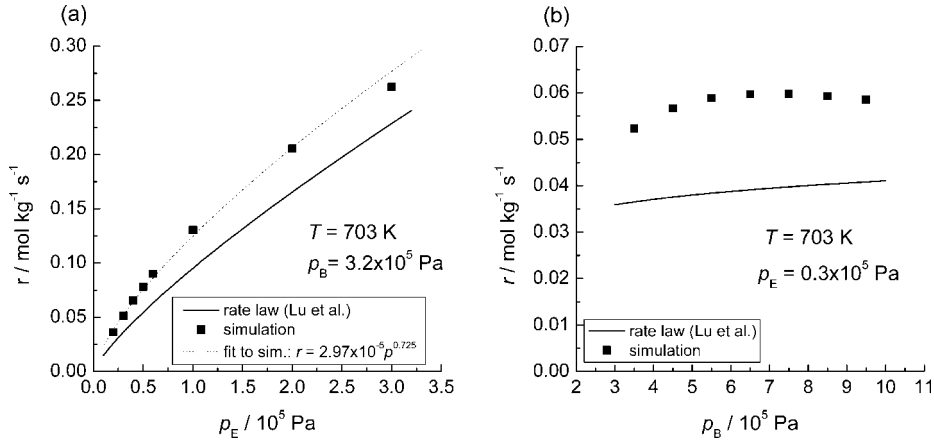

Figure 8. Simulated and experimental rates per unit mass of catalyst for the alkylation of benzene with ethene. (a) Constant benzene partial pressure of 3.2×10^5 Pa at 703 K; (b) constant ethene partial pressure of 0.3×10^5 Pa at 703 K. The partial pressure of ethylbenzene was fixed to 35 Pa. The experimental data were calculated using the rate expression of Lu et al.[46]

TABLE 4: Experimentally Determined Rate Parameters for the Power Law Rate Expression of Lu et al.[46,a]

n_E	n_B	n_{EB}	k_{10} [mol kg_{cat}^{-1} s^{-1} $Pa^{-0.905}$]	k_{20} [mol kg_{cat}^{-1} s^{-1} $Pa^{-0.276}$]	E_1 [kJ mol^{-1}]	E_2 [kJ mol^{-1}]
0.795	0.110	0.276	1.035×10^{-4}	1.281×10^{-1}	21.735	37.304

[a] The rate expression has the form $r = k_1 p_E^{n_E} p_B^{n_B} - k_2 p_{EB}^{n_{EB}}$. The rate coefficients k_i are calculated according to $k_i = k_{i0} \exp(-E_i/RT)$.

of the reaction rate from the use of a Langmuir−Hinshelwood rate expression to fit the data.

Diffusion limitation affects the reaction rates significantly. Figure 7a shows the results of simulations at constant benzene partial pressure (3.2×10^5 Pa) and increasing ethene partial pressure at 653 K. Also shown are experimental data generated using the rate law of Lu et al.[46] The diffusion coefficients reported in Table 2 were employed for the simulations. A particle diameter of 2 μm was used. In order to match the experimental data some assumptions about the porosity of the catalyst used for the experimental studies had to be made (see Appendix F of the Supporting Information for details). It was also necessary to assume the number of acid sites per unit cell since this number was not reported by Lu et al.[46] As can be seen from Figure 7a good agreement with the experimental data is achieved assuming 1.1 acid sites per unit cell. The simulations were carried out for various ethene partial pressures at a constant benzene partial pressure of 3.2×10^5 Pa and a constant ethylbenzene partial pressure of 35 Pa. Fitting the simulated points to a power law of the form $r = Ap_E^n$ gave an exponent of 0.77, in good agreement with the experimental value ($n = 0.795$). Figure 7b shows the rate of reaction as a function of the benzene partial pressure at 653 K for constant ethene and ethylbenzene partial pressures of 0.3×10^5 Pa and 35 Pa, respectively. While the absolute numbers are in reasonable agreement, the simulations predict a decrease in the reaction rate with increasing benzene partial pressure, whereas the rate law predicts a slight increase. A comparison of our model with experimental measurement of the rate of reaction for a higher benzene partial pressure (see Figure SG2a) and higher ethene partial pressure (see Figure SG2b) are presented in the Supporting Information. The agreement for the dependence of the rate on ethene partial pressure is again good. For the benzene partial pressure dependence the agreement is better than in Figure 7b. The simulations again predict a maximum in the reaction rate with increasing benzene partial pressure.

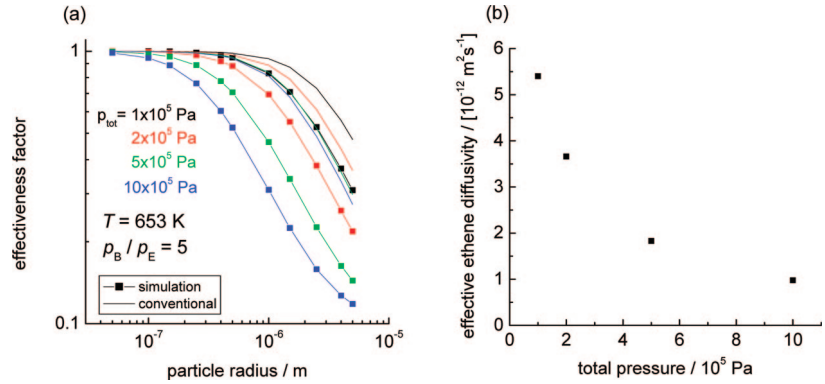

Figure 9. (a) Effectiveness factor as function of the particle radius for different gas phase pressures at 653 K and a benzene to ethene ratio of 5. (b) Effective ethene diffusivity as function of the total gas phase pressure.

At 703 K, only a qualitative comparison between the simulation and the experimental data is possible because of the very small apparent activation energy appearing in the rate law of Lu et al.[46] (see above). Because our simulations match the experimental data at 653 K they will necessarily predict higher reaction rates at 703 K. Figure 8a shows the rate of reaction at 703 K as a function of the ethene partial pressure for constant benzene partial pressure of 3.2×10^5 Pa and a constant ethylbenzene partial pressure of 35 Pa. The rate law of Lu et al.[46] predicts lower values as expected. However, the reaction order with respect to the ethene partial pressure ($n_E = 0.72$) agrees well with the experimental data. Figure 8b shows the simulated rate of reaction as function of the benzene partial pressure at 703 K for constant ethene partial pressure of 0.3×10^5 Pa and a constant ethylbenzene partial pressure of 35 Pa. The simulations again predict a higher activity. Similar results were obtained for higher benzene or ethene pressures, respectively (see Figure SG3 in the Supporting Information). It should be emphasized that the benzene partial pressure has an influence on the reaction orders with respect to ethene. At 653 K and a fixed benzene partial pressure of 10×10^5 Pa, the order is 0.87 compared to the order of 0.77 for a benzene partial pressure of 3.2×10^5 Pa. At 703 K and a fixed benzene partial pressure of 10×10^5 Pa, the order is 0.83, compared to the order of 0.72 for a benzene partial pressure of 3.2×10^5 Pa.

4.3. Effectiveness Factor. The conventional analysis of the influence of diffusional limitations on the rate for heterogeneously catalyzed reactions is often based on the assumptions of a pseudo first-order irreversible reaction and an effective diffusivity for the limiting reactant that is concentration independent. In the case of benzene alkylation with ethene the limiting reactant is usually ethene; therefore, the pseudo first-order kinetics can be written as

$$r = k_{app} C_E = k_{app} \frac{p_E}{RT} \tag{27}$$

here k_{app} is the pseudo first-order rate coefficient and C_E denotes the gas phase concentration of ethene. The Thiele modulus can be expressed as

$$\phi = \frac{R}{3} \sqrt{\frac{k_{app} \rho_{ZSM-5}}{D_{E,eff}}} \tag{28}$$

where ρ_{ZSM-5} is the zeolite density, $D_{E,eff}$ is the effective diffusivity of ethene, and R is the crystal radius (spherical geometry). The apparent first-order rate coefficient can be obtained directly from the simulated rate of reaction evaluated at the exterior surface of the crystal from eq 27. Evaluation of the effective diffusivity of ethene is less obvious. If the assumptions underlying the conventional analysis were valid, the zero-loading M-S diffusivity, $Đ_E(0)$, would be a reasonable choice. For a spherical particle, the effectiveness factor can then be obtained from

$$\eta = \frac{1}{\phi}\left(\frac{1}{\tanh(3\phi)} - \frac{1}{3\phi}\right) \tag{29}$$

The conventional analysis of mass transfer effects has been shown to lead to substantial errors for cases of strongly confined molecules.[23,24,86] Figure 9a shows plots of η versus particle radius for a temperature of 653 K, a p_B/p_E ratio of 5, and total pressures ranging from 1×10^5 to 10×10^5 Pa obtained from rigorous simulations and of the effectiveness factors obtained from a conventional analysis using the zero-loading diffusivity of ethene to calculate the classical Thiele modulus. It is seen that the simulated values of η decreases significantly as the total pressure increases for a fixed particle size. The curve for the conventional analysis is resembled only at very low pressure. From these results it can be concluded that a conventional analysis is meaningful only if the diffusivities are measured at reaction conditions. Only then can the classical formulas be used to estimate the critical particle size to avoid extensive diffusion limitation. To extract the values of effective diffusivities from the simulations we can force-fit eq 5 into the form of Fick's law for each species, that is,

$$N_i = -\rho q_{i,sat} D_{i,eff} \nabla \theta_i \tag{30}$$

where the effective Fick diffusivities of component i is a function of both, the elements of the matrix $[\Delta]$ and the gradients $\nabla\theta_i$ of all species (see ref 87). The effective ethene diffusivities obtained from eq 30 are shown in Figure 9b as function of the total gas phase pressure. They decrease by a factor of 5.5 as the pressure increases from 1×10^5 to 10×10^5 Pa. Only if these effective diffusivities are used in the conventional analysis can reasonable agreement be achieved with the rigorous simulations. It is noted that the effective diffusivities depend only weakly on the position inside the zeolite crystal. The strongest decrease is observed for 10×10^5 Pa gas phase pressure. However, in this case the effective diffusivity at the particle center is still 89% of its value at the particle exterior surface. While the simulation results shown in Figure 9a were obtained at conditions found at the reactor inlet, we also calculated the effectiveness factor for higher ethylbenzene pressure in the gas phase, corresponding to 10% conversion. The values of the effectiveness factor lie slightly above those obtained at the inlet conditions.

5. Conclusions

The influence of adsorption thermodynamics and diffusion limitation on the alkylation of benzene with ethene over H-ZSM-5 has been analyzed by means of a continuum model based on the Maxwell-Stefan (M-S) equations in combination with the ideal adsorbed solution theory (IAST). All parameters needed to solve the resulting system of differential equations have been determined from molecular simulations and quantum chemical calculations. The macroscopic behavior of two different reaction schemes, a one-step scheme and a two-step scheme, has been studied. For both schemes, a model has been proposed to describe the intrinsic rate of reaction as a function of the local concentration of reactants at the active site. It has been demonstrated that the apparent rate coefficients and the orders in the partial pressures of the reactants are not constant but, in fact, a complex function of the zeolite architecture, particle size, and reaction conditions. As a result, the widely used empirical power laws and Langmuir−Hinshelwood expressions become inappropriate when used to correlate rate data over a broad range of conditions. Moreover, the usual approaches to calculate effectiveness factors for reactions in porous media can only be used at low loadings of the reactants inside the zeolite. In fact, the effectiveness factor depends strongly on the reaction conditions. The adopted simulation model can be used to predict the effectiveness factor for any set of reaction conditions.

Acknowledgment. The present work was supported by the Deutsche Forschungsgemeinschaft (DFG) in priority program SPP 1155, the Fonds der chemischen Industrie, the Methane Conversion Cooperative supported by BP, and the Max-Buchner Forschungsstiftung.

Nomenclature

Latin Letters

A: pre-exponential factor in Arrhenius ansatz, s^{-1}
a_i: constants describing self-exchange in eq 11, dimensionless
a: Reed−Ehrlich parameter, dimensionless
$[B]$: inverse of matrix $[\Delta]$, Eq. 6, m^{-2} s
b_i: Langmuir affinity constants, Pa^{-1}
b: Reed−Ehrlich parameter, dimensionless
C_i: gas phase concentration of species i, mol m^{-3}
$D_{i,self}$: self-diffusivity, m^2 s^{-1}
$Đ_i$: Maxwell−Stefan diffusivity of species i, m^2 s^{-1}
$Đ_i(0)$: zero-loading M-S diffusivity of species i, m^2 s^{-1}
$Đ_{ii}$: self-exchange diffusivity, m^2 s^{-1}
$Đ_{ij}$: binary exchange diffusivity, m^2 s^{-1}
E: activation energy, J mol^{-1}
f_i: fugacity of species i, Pa
f: Reed−Ehrlich parameter, dimensionless
k: reaction rate coefficient, s^{-1}
k_{app}: apparent first order reaction rate coefficient, m^3 kg^{-1} s^{-1}
N_i: molar flux of species i, mol m^{-2} s^{-1}
n: number of species
n_i: exponent of species i in power law rate expression, dimensionless
p: pressure, Pa
q_i: molar loading of species i, mol kg^{-1}
$q_{i,sat}$: saturation loading of species i, mol kg^{-1}
R: gas constant, 8.314 J mol^{-1} K^{-1}; radius, m
r: rate of reaction, mol m^{-3} s^{-1}
T: absolute temperature, K
t: time, s
x_i: fraction of total loading present on site i, dimensionless
y_i: gas phase mole fraction of species i, dimensionless
z: coordination number, dimensionless

Greek Letters

β_i: Reed−Ehrlich parameter, dimensionless
Γ_{ij}: thermodynamic factor, dimensionless
γ: number of protons per unit cell
$[\Delta]$: matrix of Maxwell−Stefan diffusivities, m^2 s^{-1}
ε: Reed−Ehrlich parameter, dimensionless
η: effectiveness factor, dimensionless
θ: total occupancy of mixture, dimensionless
θ_i: fractional occupancy of component i, dimensionless
λ: average number of acid sites per intersection
μ_i: molar chemical potential, J mol^{-1}
ν_i: stoichiometric coefficient of species i, dimensionless
ξ: diffusion path, m
ρ: density of zeolite, kg m^{-3}
ø: Thiele modulus, dimensionless

Subscripts

app: referring to apparent quantity
B: benzene
eff: referring to effective quantity
E: ethene
EB: ethylbenzene
eth: ethoxide
E,H+: ethene adsorbed on acid site
E+B,H+: ethene plus benzene adsorbed on acid site
EB,H+: ethylbenzene adsorbed on acid site
eth+B: benzene adsorbed next to ethoxide
i, j: components in mixture
sat: referring to saturation conditions

Vector and Matrix Notation

(): vector
[ ]: square matrix

Supporting Information Available: This material includes a description of the simulation methodologies and force fields used as well as details on the fitting of adsorption isotherms and determination of M-S diffusivities from MD data. Moreover, it contains information on the derivation of rate expressions, the solution of the diffusion-reaction equation, the comparison between experimental and simulated rates, and additional simulation data. This material is available free of charge via the Internet at http://pubs.acs.org.

References and Notes

(1) Dwyer, F. G.; Lewis, P. J.; Schneider, F. H. *Chem. Eng.* **1976**, *83*, 90.
(2) Haag, W. O., Olson, D. H., Weisz, P. B. Shape-selective catalysis in aromatics processing. In *Chemistry for the Future*, Proceedings of the 29th IUPAC Congress; Grünewald, H., Ed.; Pergamon Press: Oxford, 1984; p 327.
(3) Weitkamp, J. *Acta Phys. Chem.* **1985**, *31*, 271.
(4) Christensen, C. H.; Johannsen, K.; Schmidt, I.; Christensen, C. H. *J. Am. Chem. Soc.* **2003**, *125*, 13370.
(5) Christensen, C. H.; Johannsen, K.; Törnquist, E.; Schmidt, I.; Topsøe, H.; Christensen, C. H. *Catal. Today* **2007**, *128*, 117.
(6) Lukyanov, D. B.; Vazhnova, T. *J. Mol. Catal. A: Chem.* **2008**, *279*, 128.
(7) Lukyanov, D. B.; Vazhnova, T. *J. Catal.* **2008**, *257*, 382.
(8) Theodorou, D.; Wei, J. *J. Catal.* **1983**, *83*, 205.
(9) Frank, B.; Dahlke, K.; Emig, G.; Aust, E.; Broucek, R.; Nywlt, M. *Microporous Mater.* **1993**, *1*, 43.

(10) Hinderer, J.; Keil, F. J. *Chem. Eng. Sci.* **1996**, *51*, 2667.
(11) Trout, B. L.; Chakraborty, A. K.; Bell, A. T. *Chem. Eng. Sci.* **1997**, *52*, 2265.
(12) Stoltze, P. *Prog. Surf. Sci.* **2000**, *65*, 65.
(13) Keil, F. J.; Coppens, M.-O. Dynamic Monte Carlo Simulations of Diffusion and Reaction in Zeolites. In *Computer Modelling of Microporous Materials*; Catlow, C. R. A., van Santen, R. A., Smit, B., Eds,; Elsevier: London, 2004; p 109.
(14) Krishna, R.; van Baten, J. M. *Microporous Mesoporous Mater.* **2008**, *109*, 91.
(15) Krishna, R.; van Baten, J. M. *Chem. Eng. Sci.* **2008**, *63*, 3120.
(16) Krishna, R.; Paschek, D. *Chem. Eng. J.* **2002**, *87*, 1.
(17) Krishna, R.; Baur, R. *Sep. Purif. Technol.* **2003**, *33*, 213.
(18) Krishna, R.; van Baten, J. M. *J. Phys. Chem. B* **2005**, *109*, 6386.
(19) Iyengar, V.; Coppens, M.-O. *Chem. Eng. Sci.* **2004**, *59*, 4747.
(20) Coppens, M.-O.; Iyengar, V. *Nanotechnology* **2005**, *16*, S442.
(21) Thiele, E. W. *Ind. Eng. Chem.* **1939**, *31*, 916.
(22) Jüttner, F. *Z. Phys. Chem.* **1909**, *65*, 595.
(23) Baur, R.; Krishna, R. *Chem. Eng. J.* **2004**, *99*, 105.
(24) Baur, R.; Krishna, R. *Catal. Today* **2005**, *105*, 173.
(25) Krishna, R.; Baur, R. *Chem. Eng. Sci.* **2005**, *60*, 1155.
(26) Myers, A. L.; Prausnitz, J. M. *AIChE J.* **1965**, *11*, 121.
(27) Köstner, M.; Klemm, E.; Emig, G. *Stud. Surf. Sci. Catal.* **2004**, *154*, 2096.
(28) Aris, R. *The Mathematical Theory of Diffusion and Reaction in Permeable Catalysts*; Clarendon Press: Oxford, 1975.
(29) Krishna, R.; Paschek, D.; Baur, R. *Microporous Mesoporous Mater.* **2004**, *76*, 233.
(30) Krishna, R.; van Baten, J. M.; García-Pérez, E.; Calero, S. *Ind. Eng. Chem. Res.* **2007**, *46*, 2974.
(31) Skoulidas, A. I.; Sholl, D. S.; Krishna, R. *Langmuir* **2003**, *19*, 7977.
(32) Krishna, R.; van Baten, J. M.; Dubbeldam, D. *J. Phys. Chem. B* **2004**, *108*, 14820.
(33) Vlugt, T. J. H.; Krishna, R.; Smit, B. *J. Phys. Chem. B* **1999**, *103*, 1102.
(34) Huang, Y.; Havenga, E. A. *J. Phys. Chem. B* **2000**, *104*, 5084.
(35) Goyal, R.; Fitch, A. N.; Jobic, H. *J. Phys. Chem. B* **2000**, *104*, 2878.
(36) Huang, Y.; Havenga, E. A. *Chem. Mater.* **2001**, *13*, 738.
(37) Floquet, N.; Coulomb, J. P.; Weber, G.; Bertrand, O.; Bellat, J. P. *J. Phys. Chem. B* **2003**, *107*, 685.
(38) Song, L.; Sun, Z. L.; Ban, H. Y.; Dai, M.; Rees, L. V. C. *Adsorption* **2005**, *11*, 325.
(39) Paschek, D.; Krishna, R. *Phys. Chem. Chem. Phys.* **2000**, *2*, 2389.
(40) Chmelik, C.; Heinke, L.; Kärger, J.; Schmidt, W.; Shah, D. B.; van Baten, J. M.; Krishna, R. *Chem. Phys. Lett.* **2008**, *459*, 141.
(41) Reed, D. A.; Ehrlich, G. *Surf. Sci.* **1981**, *102*, 588.
(42) Hansen, N.; Brüggemann, T.; Bell, A. T.; Keil, F. J. *J. Phys. Chem. C* **2008**, *112*, 15402.
(43) Krishna, R.; Baur, R. *Diffusion, Adsorption and Reaction in Zeolites: Modelling and Numerical Issues*; University of Amsterdam: Amsterdam, 2002 (http://www.science.uva.nl/research/cr/zeolite/).
(44) Do, D. D. *Adsorption Analysis: Equilibria and Kinetics*; Imperial College Press: London, 1998.
(45) Jacobsen, C. J. H.; Madsen, C.; Houzvicka, J.; Schmidt, I.; Carlsson, A. *J. Am. Chem. Soc.* **2000**, *122*, 7116.
(46) Lu, M.; Wu, Y.; Zhu, Z.; Sun, H.; Chen, Q. *Petrochem. Technol. (China)* **2001**, *30*, 182.
(47) Caro, J.; Bülow, M.; Schirmer, W.; Kärger, J.; Heink, W.; Pfeifer, H.; Zdanov, S. P. *J. Chem. Soc., Faraday Trans. 1* **1985**, *81*, 2541.
(48) Van-Den-Begin, N.; Rees, L. V. C.; Caro, J.; Bülow, M. *Zeolites* **1989**, *9*, 287.
(49) Snurr, R. Q.; Hagen, A.; Schwarz, H. B.; Ernst, S.; Weitkamp, J.; Kärger, J. *J. Catal.* **1996**, *163*, 130.
(50) Chong, S.; Jobic, H.; Plazanet, M.; Sholl, D. S. *Chem. Phys. Lett.* **2005**, *408*, 157.
(51) Bülow, M.; Schlodder, H.; Rees, L. V. C.; Richards, R. E. *Stud. Surf. Sci. Catal.* **1986**, *28*, 579.
(52) Hayhurst, D. T.; Paravar, A. *Zeolites* **1988**, *8*, 27.
(53) Wu, P.; Debebe, A.; Ma, Y. H. *Zeolites* **1983**, *3*, 118.
(54) Nayak, V. S.; Riekert, L. *Acta Phys. Chem.* **1985**, *31*, 157.
(55) Prinz, D.; Riekert, L. *Ber. Bunsenges. Phys. Chem.* **1986**, *90*, 413.
(56) Zikanova, A.; Bülow, M.; Schlodder, H. *Zeolites* **1987**, *7*, 115.
(57) Shah, D. B.; Hayhurst, D. T.; Evanina, G.; Guo, C. J. *AIChE J.* **1988**, *34*, 1713.
(58) Shen, D. M.; Rees, L. V. C. *Zeolites* **1991**, *11*, 666.
(59) Ruthven, D. M.; Eic, M.; Richards, E. *Zeolites* **1991**, *11*, 647.
(60) Hashimoto, K.; Masuda, T.; Muratami, N. *Stud. Surf. Sci. Catal.* **1991**, *69*, 477.
(61) Xiao, J.; Wei, J. *Chem. Eng. Sci.* **1992**, *47*, 1123.
(62) Xiao, J.; Wei, J. *Chem. Eng. Sci.* **1992**, *47*, 1143.
(63) Niessen, W.; Karge, H. G.; Jozefowicz, L. *Stud. Surf. Sci. Catal.* **1993**, *80*, 475.
(64) Masuda, T.; Hashimoto, K. *Stud. Surf. Sci. Catal.* **1994**, *83*, 225.
(65) Hufton, J. R.; Ruthven, D. M.; Danner, R. P. *Microporous Mater.* **1995**, *5*, 39.
(66) Roque-Malherbe, R.; Wendelbo, R.; Mifsud, A.; Corma, A. *J. Phys. Chem.* **1995**, *99*, 14064.
(67) Masuda, T.; Fujikata, Y.; Nishida, T.; Hashimoto, K. *Microporous Mesoporous Mater.* **1998**, *23*, 157.
(68) Fujikata, Y.; Masuda, T.; Ikeda, H.; Hashimoto, K. *Microporous Mesoporous Mater.* **1998**, *21*, 679.
(69) Jobic, H.; Bee, M.; Pouget, S. *J. Phys. Chem. B* **2000**, *104*, 7130.
(70) Brandani, S.; Jama, M.; Ruthven, D. *Microporous Mesoporous Mater.* **2000**, *35*−*36*, 283.
(71) Loos, J. W. P.; Verheijen, P. J. T.; Moulijn, J. A. *Chem. Eng. Sci.* **2000**, *55*, 51.
(72) Song, L.; Rees, L. V. C. *Microporous Mesoporous Mater.* **2000**, *35*−*36*, 301.
(73) Song, L.; Sun, Z.-L.; Rees, L. V. C. *Microporous Mesoporous Mater.* **2002**, *55*, 31.
(74) Song, L.; Sun, Z.-L.; Ban, H.-Y.; Dai, M.; Rees, L. V. C. *Phys. Chem. Chem. Phys.* **2004**, *6*, 4722.
(75) Karge, H. G. C. R. *Chimie* **2005**, *8*, 303.
(76) Song, L.; Sun, Z.-L.; Duan, L.; Gui, J.; McDougall, G. S. *Microporous Mesoporous Mater.* **2007**, *104*, 115.
(77) Nakasaka, Y.; Tago, T.; Odate, K.; Masuda, T. *Microporous Mesoporous Mater.* **2008**, *112*, 162.
(78) Schumacher, R.; Karge, H. G. *Collect. Czech. Chem. Commun.* **1999**, *64*, 483.
(79) Rungsirisakun, R.; Nanok, T.; Probst, M.; Limtrakul, J. *J. Mol. Graphics Modell.* **2006**, *24*, 373.
(80) Fried, J. R.; Weaver, S. *Comput. Mater. Sci.* **1998**, *11*, 277.
(81) Yue, X.; Yang, X. *Langmuir* **2006**, *22*, 3138.
(82) Forester, T. R.; Smith, W. *J. Chem. Soc., Faraday Trans.* **1997**, *93*, 3249.
(83) Keil, F. J.; Hinderer, J.; Garayhi, A. R. *Catal. Today* **1999**, *50*, 637.
(84) Takaba, H.; Suzuki, T.; Nakao, S. *Fluid Phase Equilib.* **2004**, *219*, 11.
(85) Snurr, R. Q.; Bell, A. T.; Theodorou, D. N. *J. Phys. Chem.* **1994**, *98*, 11948.
(86) Ruthven, D. M. *J. Catal.* **1972**, *25*, 259.
(87) Krishna, R.; Paschek, D. *Sep. Purif. Technol.* **2000**, *21*, 111.

JP8073046

Supplementary Material to accompany:

Analysis of diffusion limitation in the alkylation of benzene over H-ZSM-5 by combining quantum chemical calculations, molecular simulations, and a continuum approach

N. Hansen [a,*], R. Krishna [b], J. M. van Baten [b], A. T. Bell [c,*], F. J. Keil [a]

[a] *Department of Chemical Engineering, Hamburg University of Technology, D-21073 Hamburg, Germany*

[b] *Van't Hoff Institute for Molecular Sciences, University of Amsterdam, 1018 WV Amsterdam, The Netherlands*

[c] *Department of Chemical Engineering, University of California, Berkeley, CA 94720-1462, USA*

Contents:

Appendix A: Simulation methodologies

1. GCMC simulation methodology

Configurational-bias Monte Carlo (CBMC) simulations have been carried out to determine the adsorption isotherms for ethane (E), benzene (B), and ethylbenzene (EB) in MFI (all silica silicalite-1) at a variety of temperatures; the crystallographic data are available elsewhere [1, 2]. We use the united atom model. The zeolite framework is considered to be rigid. We consider the CH_x groups as single, chargeless interaction centers with their own effective potentials. The beads in the chain are connected by harmonic bonding potentials. A harmonic cosine bending potential models the bond bending between three neighboring beads, a Ryckaert-Bellemans potential controls the torsion angle. Beads in a chain separated by more than three bonds interact with each other through a Lennard-Jones potential. The Lennard-Jones potentials are shifted and cut at 12 Å. The CBMC simulation details, along with the force fields have been given in detail in earlier publications [3, 4]. The simulation box consists of 2×2×3 unit cells for MFI. Periodic boundary conditions were employed. It was verified that the size of the simulation box was large enough to yield reliable data on adsorption.

Simulations for the adsorption isotherms of ethene, and benzene was carried out with the force field of Ban et al. [5]. For ethylbenzene, the force field of benzene was used as a starting point and the force field parameters for the ethyl side chain were adapted using the alkane force field parameters of Dubbeldam et al. [3, 4] as basis. The ethylbenzene molecule was assumed rigid. The CH_2 pseudo-atom is in the plane of the benzene ring, with a fixed bond of 1.54 Å connecting the CH_2 pseudo-atom to the benzene ring. The CH_3 pseudo atom is located at a distance of 1.54 Å from the CH_2 pseudo-atom. The bond angle between the aromatic ring, the CH_2 pseudo-atom and the CH_3 pseudo atom is 114 degrees. This bond angle is in a plane perpendicular to the plane containing the aromatic ring. Lorentz-Berthelot mixing rules are used to describe the interaction between the pseudo atoms of the aromatic rings and

the two pseudo atoms of the ethyl group and the zeolite atoms. The van der Waals interactions are cut and shifted at 12 Å. An Ewald summation method is used for evaluation of the charge interactions, that model the zeolite and the dipole moment of the aromatic ring.

Additionally CBMC simulations were carried out to determine the component loadings for various binary mixtures; in these simulations the partial gas phase fugacities were equal, i.e. $f_1 = f_2$.

The CBMC simulations were performed using the BIGMAC code developed by T.J.H. Vlugt [6] as basis.

2. MD simulation methodology

Diffusion is simulated using Newton's equations of motion until the system properties, on average, no longer change in time. The Verlet algorithm is used for time integration. A time step of 1 fs was used in all simulations. For each simulation, *initializing* GCMC moves are used to place the molecules in the domain, minimizing the energy. Next, follows an *equilibration* stage. These are essentially the same as the production cycles, only the statistics are not yet taken into account. This removes any initial large disturbances in the system do not affect statistics. After a fixed number of initialization and equilibrium steps, the MD simulation *production* cycles start. For every cycle, the statistics for determining the mean square displacements (MSDs) are updated. The MSDs are determined for time intervals ranging from 2 fs to 1 ns. In order to do this, an order-*N* algorithm, as detailed in Chapter 4 of Frenkel and Smit [7] is implemented. The Nosé-Hoover thermostat is applied to all the diffusing particles.

The DLPOLY code [8] was used along with the force field implementation as described in the previous section. DL_POLY is a molecular dynamics simulation package written by W.

Smith, T.R. Forester and I.T. Todorov and has been obtained from CCLRCs Daresbury Laboratory via the website.[8]

The MD simulations were carried out for a variety of molecular loadings. All simulations were carried out on clusters of PCs equipped with Intel Xeon processors running at 3.4 GHz on the Linux operating system. Each MD simulation, for a specified loading, was run for 120 h, determined to be long enough to obtain reliable statistics for determination of the diffusivities.

The self-diffusivities, $D_{\mathrm{i,self}}$, were computed by analyzing the mean square displacement of each species *i* for each of the coordinate directions:

$$D_{i,self} = \frac{1}{2n_i} \lim_{\Delta t \to \infty} \frac{1}{\Delta t} \left\langle \left(\sum_{l=1}^{n_i} \left(\mathbf{r}_{l,i}(t + \Delta t) - \mathbf{r}_{l,i}(t) \right)^2 \right) \right\rangle \tag{1}$$

In this expression n_{i} represents the number of molecules of species *i* respectively, and $\mathbf{r}_{\mathrm{l,i}}(t)$ is the position of molecule *l* of species *i* at any time *t*. Equation 1 also defines the self-diffusivity in a *n*-component mixture.

In the Maxwell-Stefan (M-S) formulation the flux of any species in a binary mixture is related to its chemical potential gradient by [9]

$$-\rho \frac{\theta_i}{RT} \frac{d\mu_i}{dx} = \sum_{\substack{j=1 \\ j \neq i}}^{n} \frac{q_j N_i - q_i N_j}{q_{i,sat} q_{j,sat} Đ_{ij}} + \frac{N_i}{q_{i,sat} Đ_i}; \quad i = 1,...n \tag{2}$$

where N_{i} is the molar flux, ρ is the zeolite framework density, q_{i} is the molar loading, $q_{\mathrm{i,sat}}$ is the saturation capacity, $d\mu_i/dx$ is the chemical potential gradient, *R* is the gas constant, *T* is the absolute temperature, $Đ_{\mathrm{i}}$ is the M-S diffusivity, and $Đ_{\mathrm{ij}}$ are the binary exchange coefficients. Conformity with the Onsager Reciprocal Relations demands that

$$q_{j,sat} Đ_{ij} = q_{i,sat} Đ_{ji} \tag{3}$$

The gradient of the chemical potentials in Eq. 2 can be related to the gradients in the loadings by defining a 2×2 dimensional matrix of thermodynamic factors [Γ]

$$\frac{q_i}{RT}\frac{d\mu_i}{dx} = \sum_{j=1}^{2}\Gamma_{ij}\frac{dq_j}{dx}; \quad \Gamma_{ij} \equiv \frac{q_i}{f_i}\frac{\partial f_i}{\partial q_j}; \quad i, j = 1,2 \tag{4}$$

The elements Γ_{ij} in Eq. 4 can be estimated, for example, using the Ideal Adsorbed Solution Theory of Myers and Prausnitz [10] and the fits of the pure component isotherm data. The fluxes N_i can be explicitly expressed as functions of the gradients in the loading

$$(N) = -\rho[\Delta][\Gamma]\frac{d(q)}{dx} \tag{5}$$

where [Δ] is a square matrix of M-S diffusivities. Compliance with the Onsager Reciprocal Relations demands that

$$q_2\Delta_{12} = q_1\Delta_{21} \tag{6}$$

The diagonal elements Δ_{ii} in each of the coordinate directions for the linear alkanes were obtained from

$$\Delta_{ii} = \frac{1}{2}\lim_{\Delta t\to\infty}\frac{1}{n_i}\frac{1}{\Delta t}\left\langle\left(\sum_{l=1}^{n_i}\left(\mathbf{r}_{l,i}(t+\Delta t) - \mathbf{r}_{l,i}(t)\right)\right)^2\right\rangle \tag{7}$$

In this expression n_i represents the number of molecules of species *i*, and $\mathbf{r}_{l,i}(t)$ is the position of molecule *l* of species *i* at any time *t*.

The values of Δ_{ii} for benzene and ethylbenzene are about 2-3 orders of magnitude lower than that of the ethene; these are too low to be accurately determined from MD simulations and are not reported in the paper.

3. Snapshots and animations

Snapshots showing the location of the molecules within the intersecting channel structures of MFI are shown in Figures 1, 2, and 3.

The intersection blocking effect in MFI by B and EB during diffusion of mixtures is best appreciated by viewing the animations of the MD simulations [11].

4. References

[1] C. Baerlocher, L.B. McCusker, Database of Zeolite Structures, International Zeolite Association, http://www.iza-structure.org/databases/, 26 June 2001.

[2] J.M. van Baten, R. Krishna, MD Simulations of Diffusion in Zeolites, University of Amsterdam, http://www.science.uva.nl/research/cr/md/,

[3] D. Dubbeldam, S. Calero, T.J.H. Vlugt, R. Krishna, T.L.M. Maesen, E. Beerdsen, B. Smit, Force Field Parametrization through Fitting on Inflection Points in Isotherms, Phys. Rev. Lett. 93 (2004) 088302.

[4] D. Dubbeldam, S. Calero, T.J.H. Vlugt, R. Krishna, T.L.M. Maesen, B. Smit, United Atom Forcefield for Alkanes in Nanoporous Materials, J. Phys. Chem. B 108 (2004) 12301-12313.

[5] S. Ban, A. van Laak, P.E. de Jongh, J.P.J.M. van der Eerden, T.J.H. Vlugt, Adsorption Selectivity of Benzene and Propene Mixtures for Various Zeolites, J. Phys. Chem. C 111 (2007) 17241-17248.

[6] T.J.H. Vlugt, BIGMAC, University of Amsterdam, http://molsim.chem.uva.nl/bigmac/, 1 November 2000.

[7] D. Frenkel, B. Smit, Understanding molecular simulations: from algorithms to applications, Academic Press, 2nd Edition, San Diego, 2002.

[8] W. Smith, T.R. Forester, I.T. Todorov, The DL_POLY Molecular Simulation Package, Warrington, England, http://www.cse.clrc.ac.uk/msi/software/DL_POLY/index.shtml, March 2006.

[9] R. Krishna, J.M. van Baten, Diffusion of alkane mixtures in zeolites. Validating the Maxwell-Stefan formulation using MD simulations, J. Phys. Chem. B 109 (2005) 6386-6396.

[10] A.L. Myers, J.M. Prausnitz, Thermodynamics of mixed gas adsorption, A.I.Ch.E.J. 11 (1965) 121-130.

[11] J.M. van Baten, R. Krishna, MD animations of diffusion in nanoporous materials, University of Amsterdam, Amsterdam, http://www.science.uva.nl/research/cr/animateMD/, 3 February 2008.

5. Captions for Figures

Figure 1. Snapshots showing the location of ethene molecules in MFI at a total loading of 4 molecules per unit cell. The molecules of 3 layers are shown in each channel.

Figure 2. Snapshots showing the location of ethene and benzene molecules in MFI at a total loading of 4 molecules per unit cell. The molecules of 3 layers are shown in each channel.

Figure 3. Snapshots showing the location of ethene and ethylbenzene molecules in MFI at a total loading of 4 molecules per unit cell. The molecules of 3 layers are shown in each channel.

6. Figures

Figure SA1

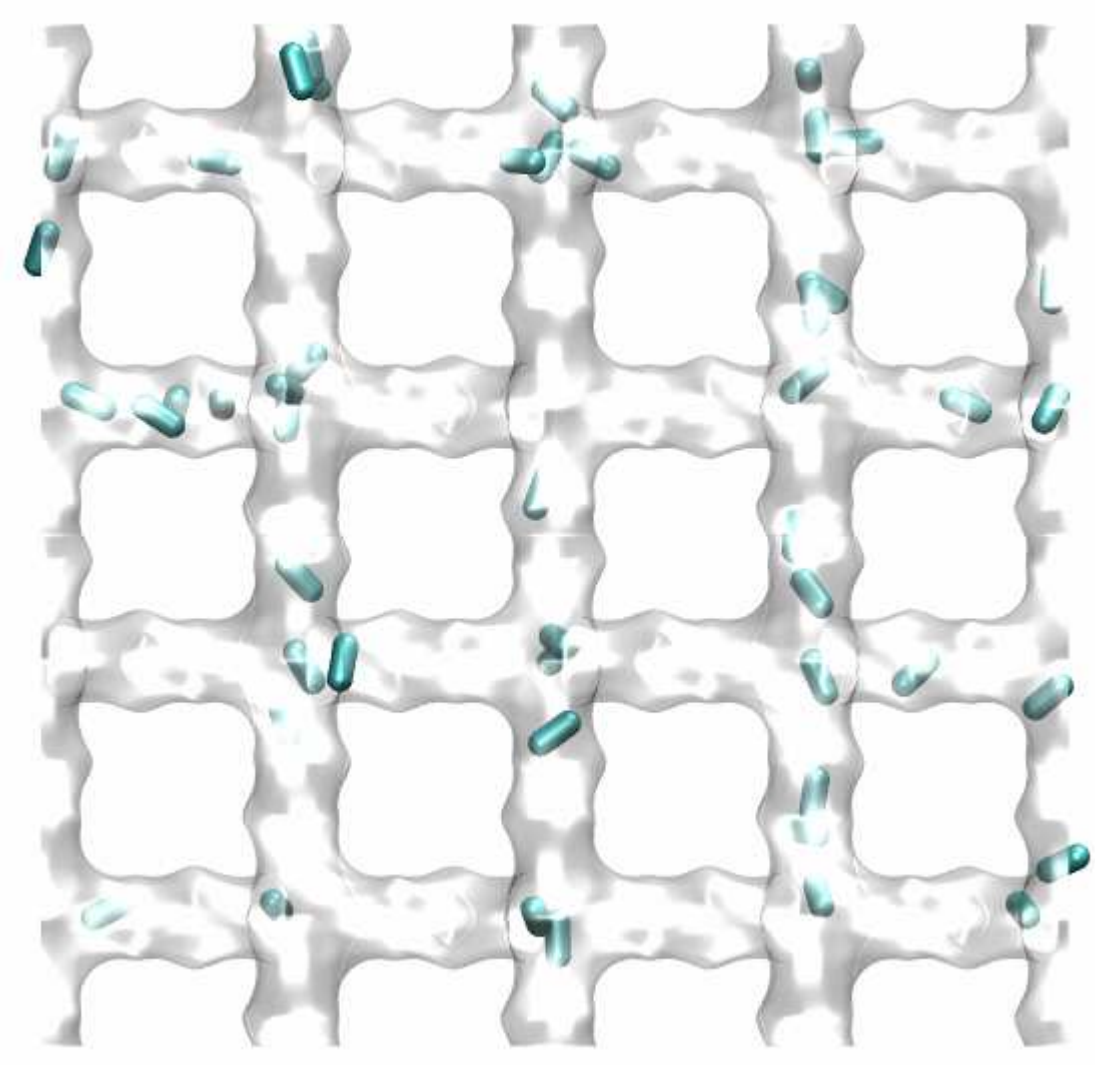

Figure SA2

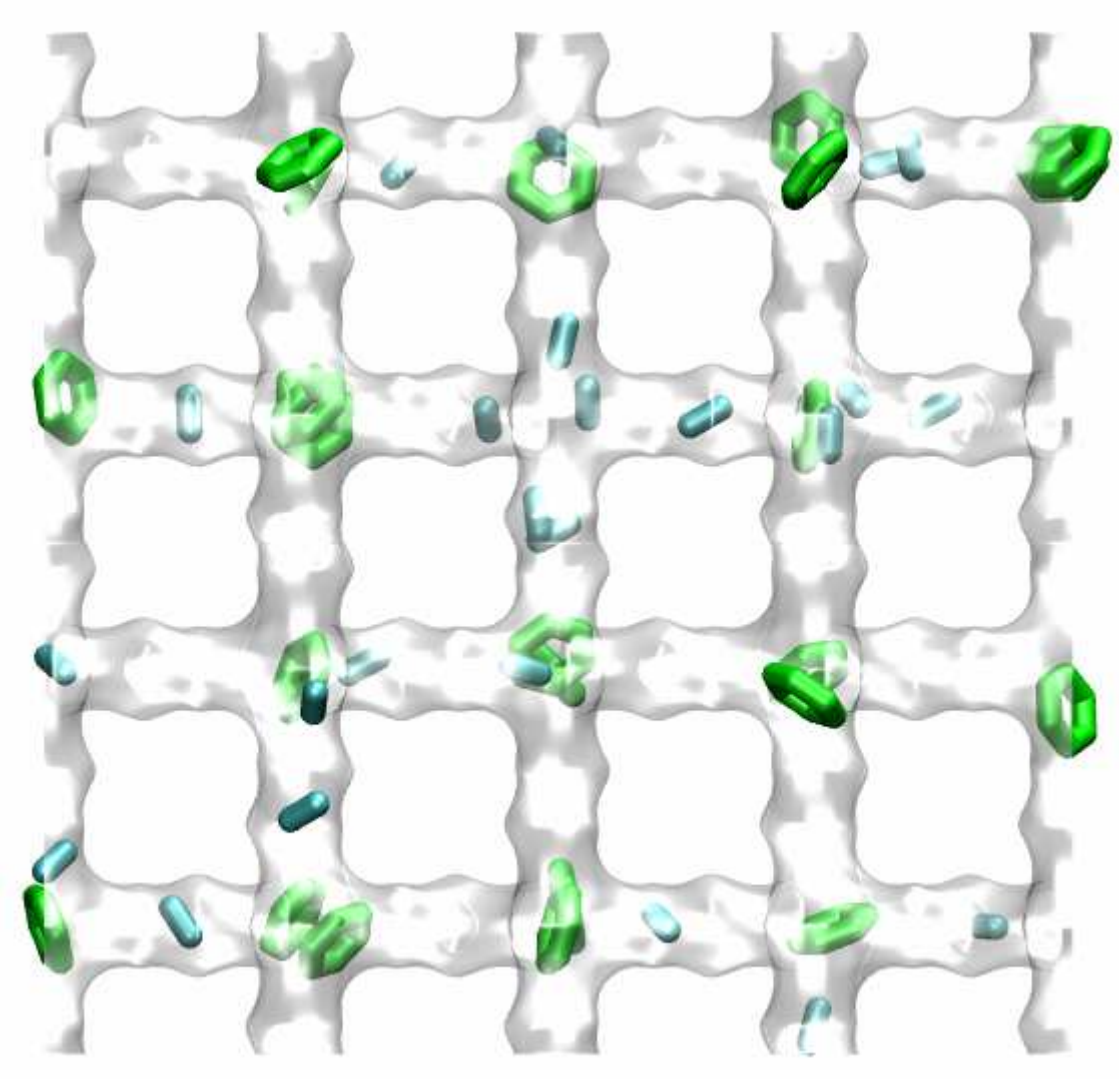

Figure SA3

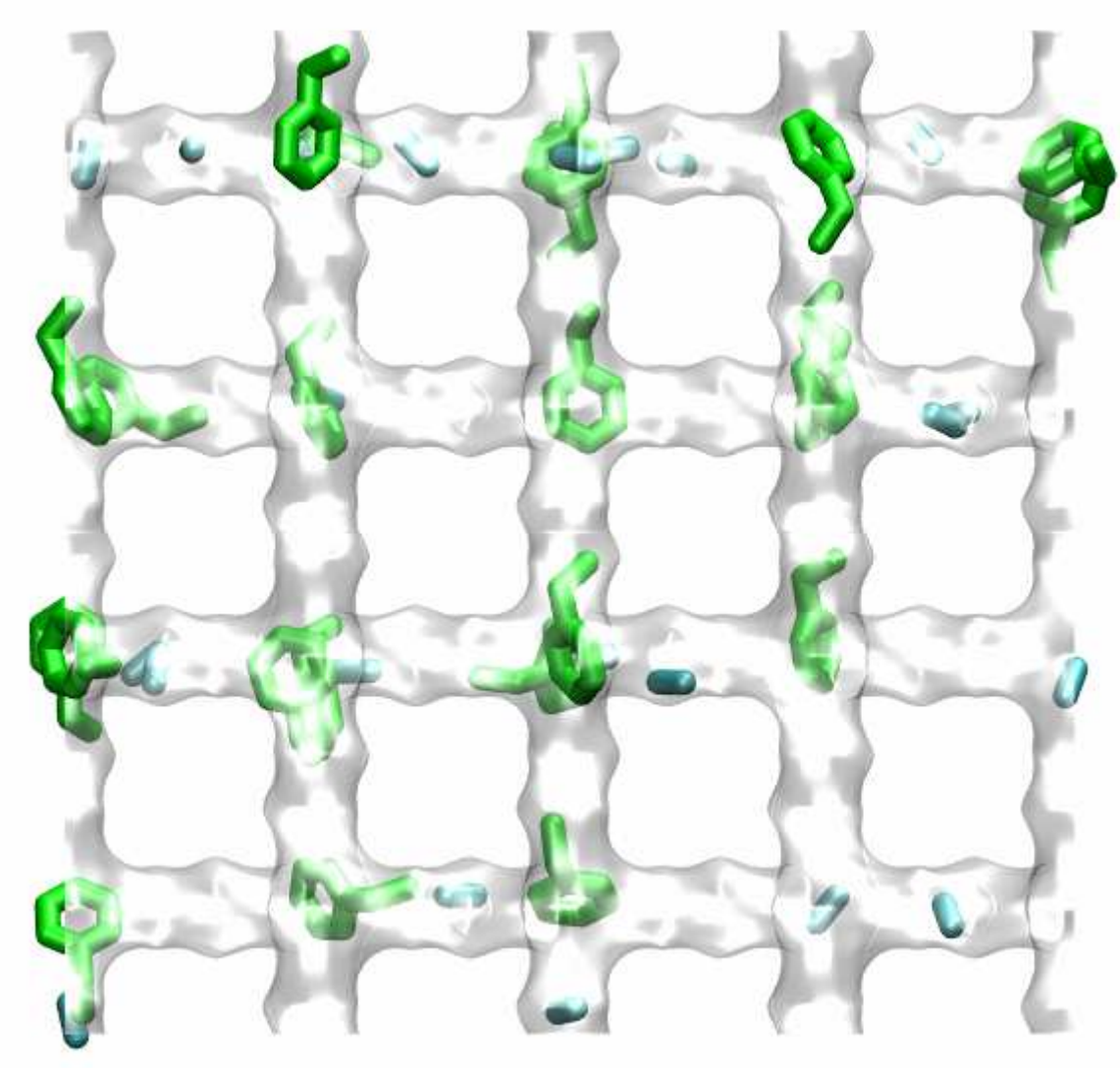

Appendix B: Fitting of adsorption isotherms for C_2H_4, C_6H_6, C_8H_{10} in MFI and validation of the ideal adsorbed solution theory.

1. Methodology

Adsorption isotherms at three different temperatures have been obtained from CBMC simulations in the grand canonical ensemble as outlined in Appendix A. The simulation data were fitted to a three site Langmuir model

$$q_i = \frac{q_{i,sat,A} b_{i,A} f_i}{1 + b_{i,A} f_i} + \frac{q_{i,sat,B} b_{i,B} f_i}{1 + b_{i,B} f_i} + \frac{q_{i,sat,C} b_{i,C} f_i}{1 + b_{i,C} f_i} \quad . \tag{1}$$

where $q_{i,sat,X}$ denotes the saturation capacity of species i on site X in molecules per unit cell, $b_{i,X}$ is the affinity constant in Pa^{-1}, and f_i is the gas phase fugacity of species i in Pa. As can be seen in Fig. SB1, the agreement between simulation and isotherm model is good over the whole range of fugacities. The values of the fit-parameters are given in Table SB1. We used the ideal adsorbed solution theory (IAST) [1] to calculate multicomponent mixture adsorption from the knowledge of the pure component adsorption isotherms. Due to segregation effects in mixture adsorption, predictions from IAST might deviate from GCMC predictions [2-4]. Therefore we compared the results from a GCMC simulation of a binary ethene-benzene mixture with equal partial fugacities adsorbed in MFI to the predictions from the IAS theory. As can be seen in Fig. SB2, both data sets agree well up to a partial gas phase fugacity of 10^6 Pa which covers the industrially relevant process conditions.

2. References

[1] A. L. Myers, J. M. Prausnitz, Thermodynamics of mixed gas adsorption, AIChE J. 11 (1965) 121–127.

[2] R. Krishna, D. Paschek, Molecular simulations of adsorption and siting of light alkanes in silicalite-1, Phys. Chem. Chem. Phys. 3 (2001) 453-462.

[3] R. Krishna, J. M. van Baten, Influence of segregated adsorption on mixture diffusion in DDR zeolite, Chem. Phys. Lett. 446 (2007) 344-349.

[4] M. Murthi and R. Q. Snurr, Effects of molecular siting and adsorbent heterogeneity on the ideality of adsorption equilibria, Langmuir 20 (2004) 2489-2497.

3. Table captions

Table SB1: Three-site Langmuir parameters for C_2H_4, C_6H_6, and C_8H_{10} in MFI. The saturation capacity q_{sat} has the unit of molecules per unit cell. The Langmuir affinity constants are given in Pa^{-1}.

4. Tables

Table SB1

		three-site Langmuir parameters					
molecule	temperature	$q_{i,sat,A}$	$b_{i,A}$	$q_{i,sat,B}$	$b_{i,B}$	$q_{i,sat,C}$	$b_{i,C}$
C_2H_4	603 K	12	1.31E-07	5	2.37E-09	2	5.58E-12
C_2H_4	653 K	12	8.40E-08	5	1.50E-09	2	4.46E-12
C_2H_4	703 K	12	5.62E-08	5	1.03E-09	2	4.26E-12
C_6H_6	603 K	4	4.15E-06	4	8.20E-09	4	1.42E-10
C_6H_6	653 K	4	1.97E-06	4	4.44E-09	4	7.58E-11
C_6H_6	703 K	4	9.76E-07	4	2.50E-09	4	4.94E-11
C_8H_{10}	603 K	4	9.24E-06	2	1.40E-09	2	9.94E-12
C_8H_{10}	653 K	4	3.13E-06	2	5.58E-10	0	0
C_8H_{10}	703 K	4	1.16E-06	2	2.11E-10	2	6.37E-12

5. Figure captions

Figure SB1: Pure component adsorption isotherms of ethene, benzene and ethylbenzene in MFI at three different temperatures. The symbols represent results from GCMC simulations. The lines are three-site Langmuir fits of the GCMC simulated isotherms.

Figure SB2: Total and partial adsorption isotherms in MFI for a ethene-benzene mixture at equal partial gas phase fugacities. The symbols represent GCMC simulations, the lines are predictions of the IAS theory.

6. Figures

Figure SB1

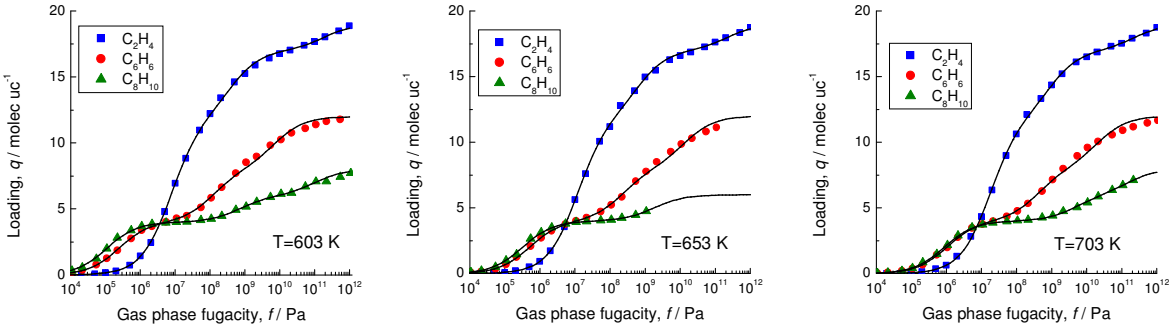

Figure SB2

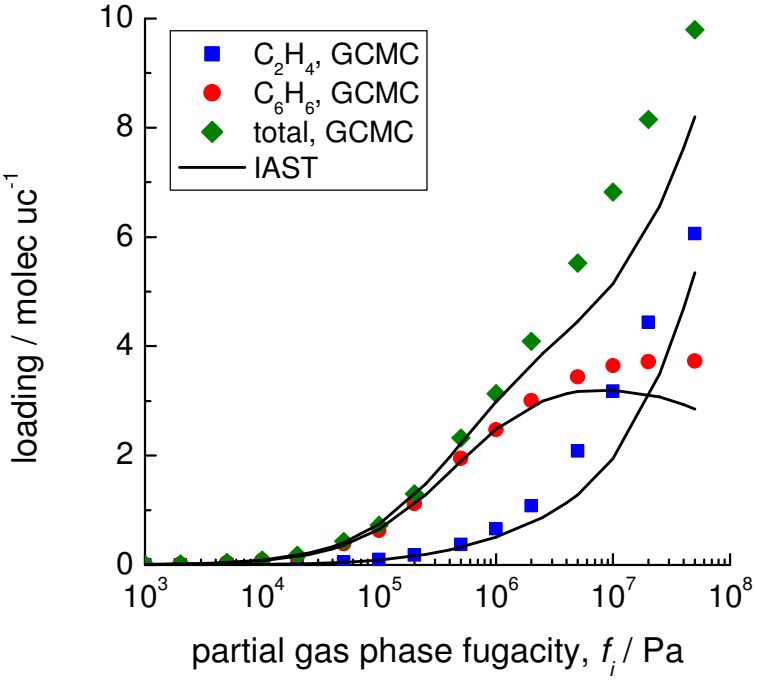

Appendix C: Extraction of M-S diffusivities from MD simulation data

1. Methodology

Diffusivity data for ethene have been obtained from MD simulations at three different temperatures. Figure SC1 (left column) shows the simulated self- and M-S-diffusivity as a function of loading along with the Reed-Ehrlich fit of the M-S-diffusivity for three different temperatures. The simulated self-exchange diffusivity is shown in the right column. It has been fitted to the analytical expression given in Eq. 11 of the main text. All fit parameters for ethene are summarized in Table SC1. The diffusivities of benzene and ethylbenzene are too small to obtain reliable results from MD simulations. However, the required zero loading M-S diffusion coefficients can be obtained indirectly by comparing predictions from the M-S equation against data from mixture MD simulations. The M-S equations lead to the following expression for the self-diffusivity of ethene (species 1) in mixtures with either benzene or ethylbenzene (species 2) [1]:

$$D_{1,self} = 1 \Big/ \left(\frac{1}{Đ_1} + \frac{\theta_1}{Đ_{11}} + \frac{\theta_2}{Đ_{12}} \right) \tag{1}$$

Equation 1 has been verified to be of good accuracy for a wide variety of alkane mixtures in different zeolites [1]. Usage of Eq. 1 requires an assumption for the M-S diffusivity of benzene (or ethylbenzene) at zero loading, $Đ_2(0)$, along with the constants in Eq. 11 of the main text. For the latter it is reasonable to use information on kMC simulations for 2-methyl-hexane (2MH) in MFI as starting point [2] because of a similar diffusion mechanism. Both the zero loading M-S diffusivity and the constants appearing in Eq. 11 of the main text can then be used as fit parameters to obtain coincidence between the predictions from the M-S

equations and the mixture MD simulations. A crucial point is the proper choice of the $q_{i,sat}$ for the calculation of the fractional occupancies in the mixture. While for ethene the maximum saturation capacity can be taken directly from MC simulations ($q_{E,sat}$ = 22 molecules per unit cell) this is not the case for benzene and ethylbenzene. Only for q_{sat} = 4 molecules per unit cell do the predictions from the M-S equation coincide with the MD results. The usage of the maximum saturation capacity from MC simulation (12 molecules per unit cell for benzene and 8 molecules per unit cell for ethylbenzene) does not lead to reasonable results. The reason is that at a loading of four molecules per unit cell all intersections are blocked and consequently the diffusive transport is virtually disrupted. The influence of preferential location of branched alkanes and benzene on the diffusion of partner molecules has been investigated both experimentally [3,4] and by using molecular dynamics [5]. There is evidence to indicate that MD simulations are able to capture the influence of intersection blocking by branched alkanes and benzene on the diffusivity of partner molecules, not only qualitatively but also reasonably quantitatively [5]. This bodes well the applicability of the MD simulations in the current study to obtain diffusivity data. The intersection blocking effect in MFI by B and EB during diffusion of mixtures is best appreciated by viewing the animations of MD simulations [6]. This behavior cannot be captured correctly when using the maximum saturation capacities for benzene and ethylbenzene, respectively. A further check will be provided by the data on the diagonal element Δ_{11} of the inverse matrix appearing in Eq. 5 of the main text. For a binary mixture Δ_{11} is related to the M-S diffusivities by [7]:

$$\Delta_{11} = \frac{Đ_1}{1+\frac{\theta_2}{1+\frac{Đ_{12}/Đ_1}{1+\frac{\theta_1}{Đ_{21}/Đ_2}}}} \qquad (2)$$

In order to evaluate Eqs 1 and 2 the following MD mixture simulation campaigns were conducted. At 653 K MD simulations of ethene-benzene mixtures with benzene loadings of 1, 2, and 3 molecules per unit cell were performed as well as simulations at total loadings of 4 molecules per unit cell. Moreover ethene-ethylbenzene mixtures with ethylbenzene loadings of 2 molecules per unit cell and total loadings of 4 molecules per unit cell were carried out. At 603 K and 703 K, MD simulations of ethene-benzene mixtures with benzene loadings of 2 molecules per unit cell and total loadings of 4 molecules per unit cell were conducted. Note that no simulations for ethene-ethylbenzene mixtures were performed at these temperatures. Instead the ratio between the zero loading diffusivities of benzene and ethylbenzene was assumed to be constant for all temperatures and taken from the results at 653 K.

Figure SC2 shows that good agreement between predictions from the M-S equations and the MD mixture data at 653 K can be achieved when setting $Đ_2(0) = 5.0\times10^{-10}$ m^2 s^{-1} for benzene and $Đ_2(0) = 4.0\times10^{-10}$ m^2 s^{-1} for ethylbenzene. The fit parameter a_1 appearing in Eq. 11 of the main text was set to 3 while a_2 to a_4 were all set to zero. Good agreement is also achieved at 603 K and 703 K (see Fig. SC3). The reason for the not so good agreement between the M-S equations and the MD data for Δ_{11} compared to $D_{1,\text{self}}$ is that (i) Δ_{11} is less accurately determined by MD as is $D_{1,\text{self}}$ and (ii) Δ_{11} depends explicitly on $Đ_2$ which is not known exactly. By contrast, $D_{1,\text{self}}$ does not explicitly depend on $Đ_2$.

2. References

[1] R. Krishna, J. M. van Baten, Diffusion of alkane mixtures in zeolites. Validating the Maxwell-Stefan formulation using MD simulations, J. Phys. Chem. B 109 (2005) 6386-6396.

[2] A. I. Skoulidas, D. S. Sholl, R. Krishna, Correlation effects in diffusion of CH4/CF4 mixtures in MFI zeolite. A study linking MD simulations with the Maxwell-Stefan formulation, Langmuir 19 (2003) 7977-7988.

[3] C. Förste, A. Germanus, J. Kärger, H. Pfeifer, J. Caro, W. Pilz, A. Zikánóvá, Molecular mobility of methane adsorbed in ZSM-5 containing co-adsorbed benzene, and the location of benzene molecules, J. Chem. Soc., Faraday Trans. 1. 83 (1987) 2301-2309.

[4] M. Fernandez, J. Kärger, D. Freude, A. Pampel, J.M. van Baten, R. Krishna, Mixture diffusion in zeolites studied by MAS PFG NMR and molecular simulation, Microporous Mesoporous Mater. 105 (2007) 124-131.
[5] R. Krishna, J.M. van Baten, Diffusion of hydrocarbon mixtures in MFI zeolite: Influence of intersection blocking, Chem. Eng. J. 140 (2008) 614-620.
[6] J. M. van Baten, R. Krishna, MD animations of diffusion in nanoporous materials, University of Amsterdam, Amsterdam, http://www.science.uva.nl/research/cr/animateMD/, 3 February 2008.
[7] R. Krishna, J. M. van Baten, Insights into diffusion of gases in zeolites gained from molecular dynamics simulations**,** Microporous Mesoporous Mater. 109 (2008) 91-108.

3. Table captions

Table SC1: Diffusion data for ethene in MFI.

Table SC2: Diffusion data for benzene and ethylbenzene in MFI.

4. Tables

Table SC1

			Reed-Ehrlich model parameters (Eqs 16, 17)			Parameters for self-exchange (Eq. 11)			
temperature [K]	q_{sat} [molec uc^{-1}]	$Đ_i(0)$ [10^{-8} m^{2}s^{-1}]	z	a	b	a1	a2	a3	a4
603	22	2.2	2.5	0.9074	0.1271	0.3135	26.79	0.4192	1.17
653	22	2.5	2.5	0.7687	0.3651	0.1088	1.4554	0.3063	0.90
703	22	2.5	2.5	0.9709	-0.0399	4.14	71.77	0.3908	0.8947

Table SC2

				Parameters for self-exchange (Eq. 11)			
molecule	temperature [K]	q_{sat} [molec uc^{-1}]	$Đ_i(0)$ [10^{-10} m^{2}s^{-1}]	a1	a2	a3	a4
C_6H_6	603	4	4.0	3	0	0	0
C_6H_6	653	4	5.0	3	0	0	0
C_6H_6	703	4	7.0	3	0	0	0
C_8H_{10}	603	4	3.2	3	0	0	0
C_8H_{10}	653	4	4.0	3	0	0	0
C_8H_{10}	703	4	5.6	3	0	0	0

6. Figure captions

Figure SC1: Diffusion data for ethene in MFI at 603, 653, and 753 K. Left column: Self and M-S diffusivity; right column: Self-exchange diffusivity.

Figure SC2: Diffusion data for ethene-benzene (top row) and ethene-ethylbenzene (bottom row) binary mixtures in MFI at 653 K. The MD simulation results (open symbols) for the self diffusivity (left figures) and the Δ_{11} element (right figures) are compared to the predictions from the M-S equations (filled symbols) at different loadings.

Figure SC3: Diffusion data for ethylene-benzene binary mixtures in MFI at 603 K (top row) and at 703 K (bottom row). The MD simulation results (open symbols) for the self diffusivity (left figures) and the Δ_{11} element (right figures) are compared to the predictions from the M-S equations (filled symbols) at different loadings.

7. Figures

Figure SC1

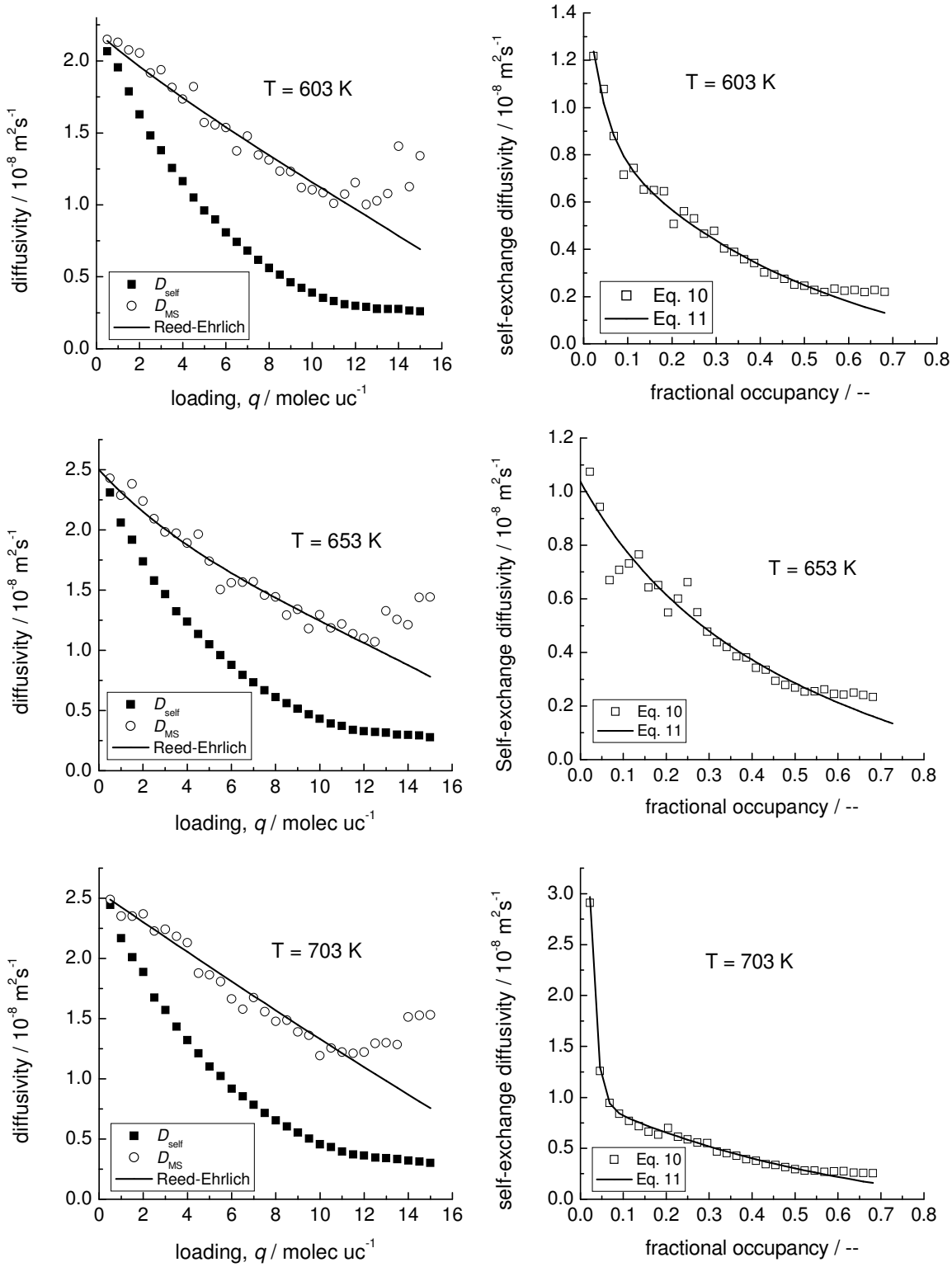

Figure SC2

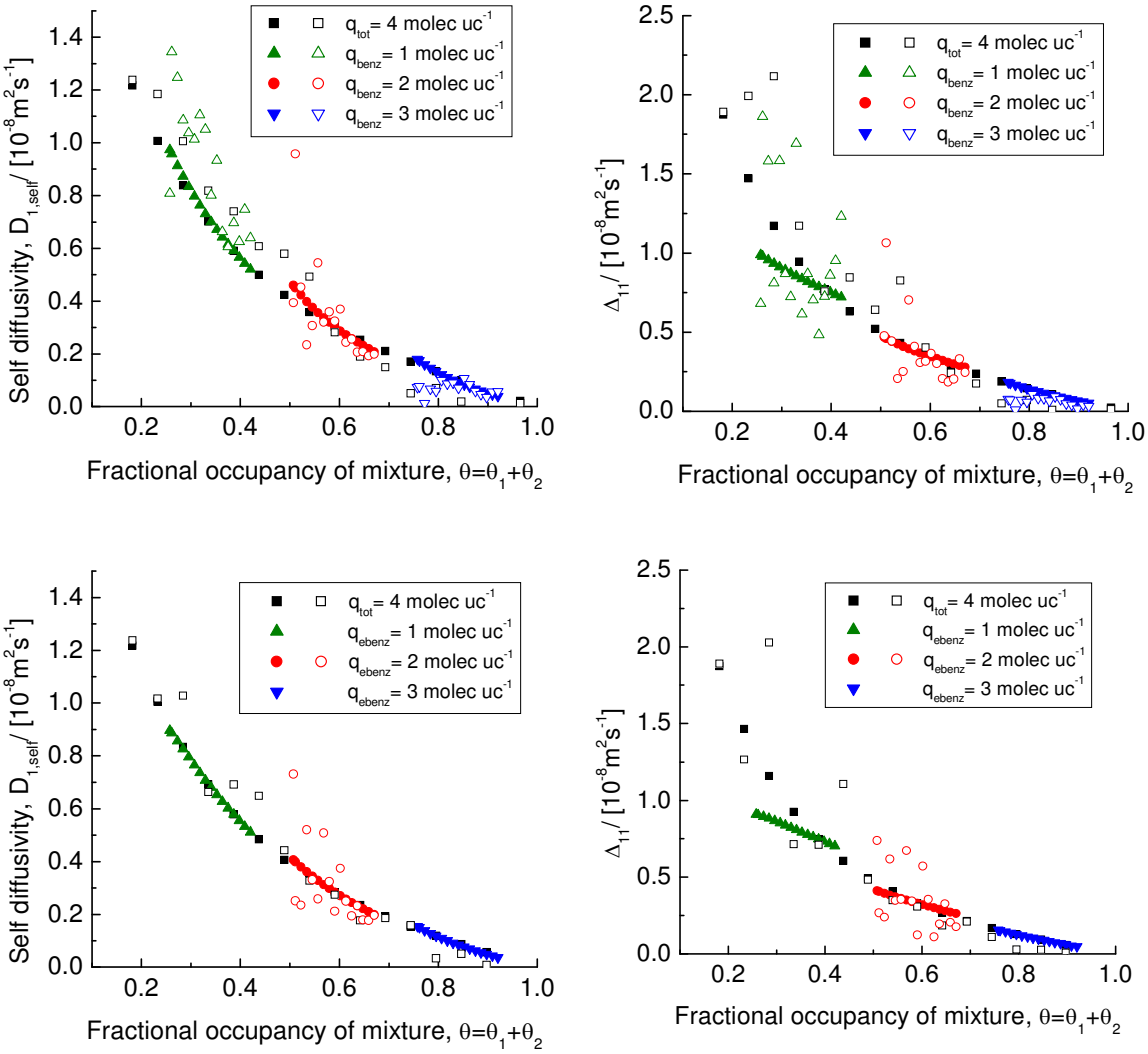
Self diffusivity, $D_{1,self}$/ [$10^{-8}m^2s^{-1}$]
Δ_{11}/ [$10^{-8}m^2s^{-1}$]
Fractional occupancy of mixture, $\theta=\theta_1+\theta_2$
q_{tot}= 4 molec uc^{-1}
q_{benz}= 1 molec uc^{-1}
q_{benz}= 2 molec uc^{-1}
q_{benz}= 3 molec uc^{-1}
q_{ebenz}= 1 molec uc^{-1}
q_{ebenz}= 2 molec uc^{-1}
q_{ebenz}= 3 molec uc^{-1}

Figure SC3

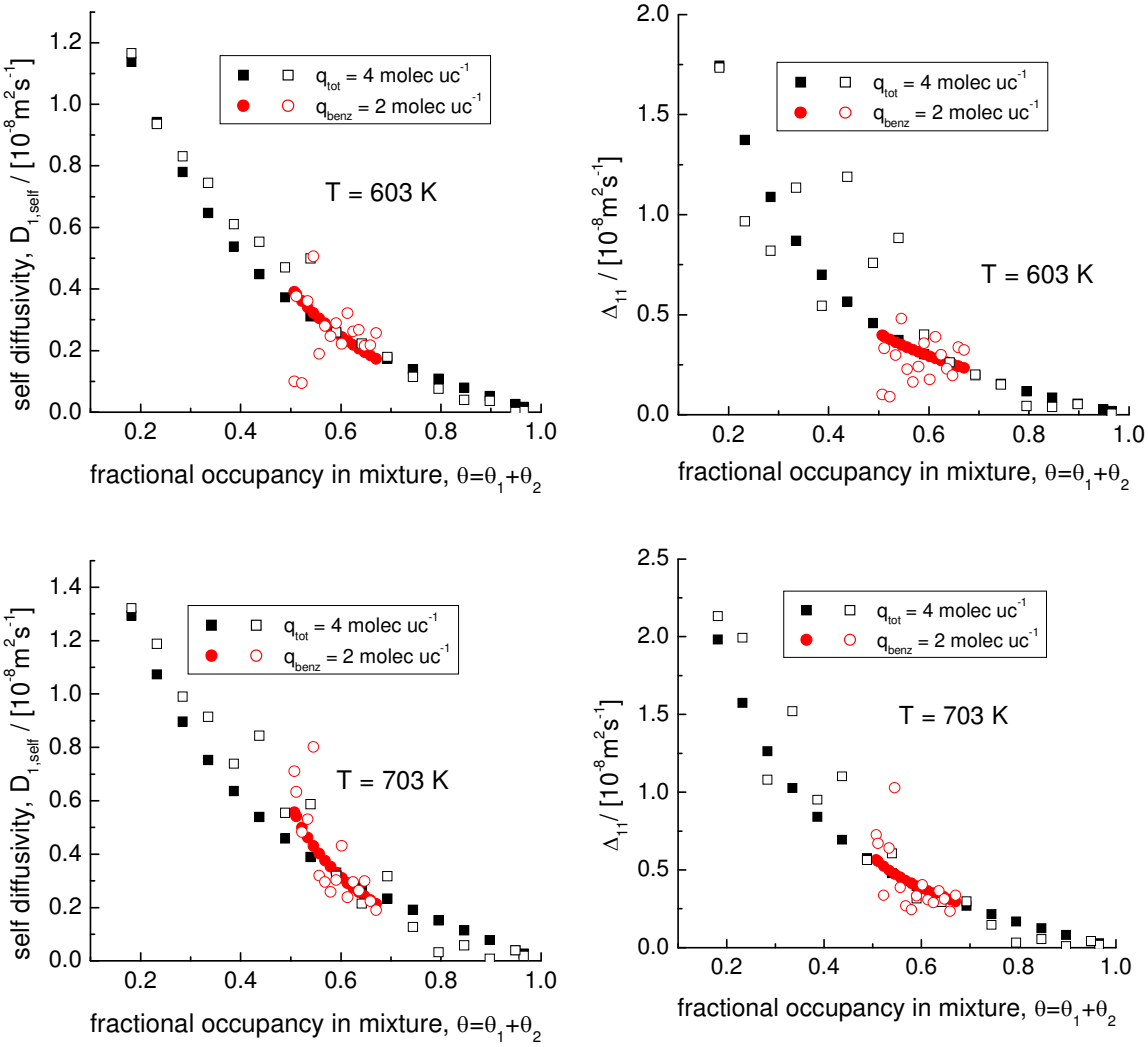
self diffusivity, $D_{1,self}$ / [10^{-8} m^2s^{-1}]
Δ_{11} / [10^{-8} m^2s^{-1}]
q_{tot} = 4 molec uc^{-1}
q_{benz} = 2 molec uc^{-1}
T = 603 K
T = 703 K
fractional occupancy in mixture, $\theta=\theta_1+\theta_2$

Appendix D: Derivation of the rate expression for the two-step alkylation

The first step in the two-step scheme is the formation of an ethoxide species via the reaction of adsorbed ethene with the Brønsted acid proton of the zeolite. The second step is the reaction of benzene adsorbed next to the ethoxide species to form ethylbenzene. The fraction of Brønsted sites occupied by ethoxide species will depend on the rate of formation and consumption of these species. The rate expression for the first step reads

$$r_{\mathrm{Eth}} = k_1 q_{\mathrm{E,H+}} - k_{-1} q_{\mathrm{Eth}} \tag{1}$$

where $q_{\mathrm{E,H+}}$ is the concentration of ethene molecules adsorbed at a Brønstedt acid site and q_{Eth} is the concentration of ethoxide species. The rate expression for the second step is

$$r_{\mathrm{EB}} = k_2 q_{\mathrm{Eth+B}} - k_{-2} q_{\mathrm{EB,H+}} \tag{2}$$

where $q_{\mathrm{Eth+B}}$ is the concentration of benzene adsorbed next to an ethoxide and $q_{\mathrm{EB,H+}}$ is the concentration of ethylbenzene located in acid site containing intersections.

Using a similar derivation of the rate expression as for the one step scheme we can express the number of adsorption sites for ethene in a mixture of ethene, benzene, ethylbenzene, and ethoxide as

$$q_{\mathrm{E,tot}} = 22 - 3.25 q_{\mathrm{B}} - 3.5 q_{\mathrm{EB}} - q_{\mathrm{Eth}} \tag{3}$$

The only difference to Eq. 20 of the main text is the additional term q_{Eth} accounting for the fact that each ethoxide reduces the number of adsorption sites for ethene by 1 (assumed). Now we need to know how many of these $q_{\mathrm{E,tot}}$ sites are located in intersections where the formation of ethoxide takes place. From MC simulations we know that the maximum ethene adsorption capacity of MFI with all intersections blocked by benzene is 9 molecules per unit cell. We can therefore estimate the ethene adsorption capacity of the intersections as 22-9 = 13 molecules per unit cell or 3.25 molecules per intersection. Each benzene and each ethylbenzene block an entire intersection i.e. reduce the number of sites available for ethene

by 3.25 molecules per unit cell. Moreover an intersection containing already an ethoxide is not available for ethoxide formation i.e. reduces the number of sites also by 3.25 molecules per unit cell. Therefore we can express the concentration of ethene molecules adsorbed at a Brønstedt acid site, $q_{E,H+}$, as

$$q_{E,H+} = \frac{13 - 3.25(q_B + q_{EB} + q_{Eth})}{22 - 3.25q_B - 3.5q_{EB} - q_{Eth}} q_E \lambda \tag{4}$$

For the second step we need to estimate the concentration of benzene adsorbed next to an ethoxide species. If we assume that benzene occupies an empty intersection with the same probability than one which contains an ethoxide, we can write for the concentration of benzene adsorbed next to an ethoxide, q_{Eth+B},

$$q_{Eth+B} = \frac{q_B}{4 - q_{EB}} q_{Eth} \tag{5}$$

The concentration of the ethoxide species is treated as unknown variable such as the concentrations of benzene, ethylbenzene, and ethene. The difference is that the diffusivity of ethoxide is zero. The exterior surface concentration of ethoxide is determined numerically by solving $r_{Eth} - r_{EB} = 0$ at the surface conditions.

Appendix E: Program structure for solving the diffusion-reaction equation

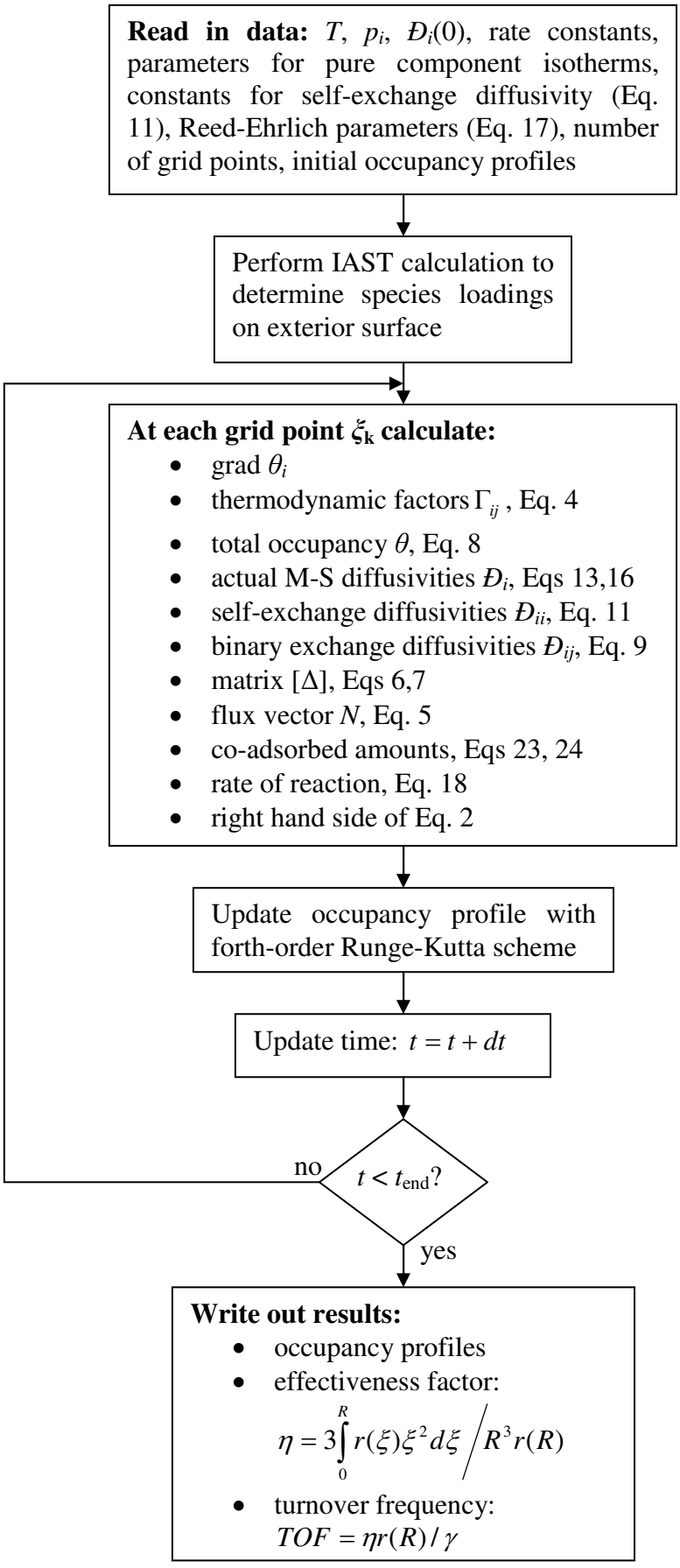

Appendix F: Conversion between simulated rates on MFI and experimental rates on zeolite AB-97™

1. Methodology

AB™ series catalysts are synthetic zeolite catalysts used for vapour phase alkylation of benzene to ethylbenzene. The AB-97™ catalyst is commercially employed in several Mobil/badger-licensed process plants in China [1]. For the bulk density of the catalyst used by Lu et al. a value of ρ_{bulk} = 600 – 700 kg m^{-3} is reported [2]. We assume that (i) the catalyst consist only of MFI (ρ = 1785.1 kg m^{-3}) and alumina (ρ = 801 kg m^{-3} [3]) and (ii) the bed porosity has a value of 0.5. Then, a bulk density of ρ_{bulk} = 646.5 kg m^{-3} is obtained in good agreement with the reported bulk density. The factor to convert simulated rates per unit mass of MFI to rates per unit mass of AB-97™ is thus f = 0.69 kg_{MFI} kg_{cat}^{-1}.

2. References

[1] http://www.sript.com.cn/er&d/er&d6-asp-m.pdf, May 14, 2008

[2] M. Lu, Y. Wu, Z. Zhu, H. Sun, Q. Chen, Ethylbenzene synthesis over AB-97 zeolite. I: The intrinsic kinetics and macrokinetics, Petrochemical Technol. (China) 30 (2001) 182–187.

[3] R. H. Perry, C. H. Chilton (Eds), Chemical Engineers' Handbook, 5th ed., McGraw-Hill, New York, 1973.

Appendix G: Additional data illustrating the influence of temperature and partial pressures on observed macroscopic reaction orders.

1. Description of data

The data presented in this section are intended to illustrate how macroscopic rate orders depend on the adsorption equilibrium of the multicomponent mixture as well as diffusional limitations. They are supporting the conclusions drawn in Section 4 of the main text.

2. Figure captions

Figure SG1: Dependence of the amount of co-adsorbed C_2H_4 + C_6H_6 on the ethene partial pressure at (a) T = 653 K and $p_B = 10\times10^5$ Pa, (c) T = 703 K and $p_B = 10\times10^5$ Pa. Dependence of the amount of co-adsorbed C_2H_4 + C_6H_6 on the benzene partial pressure at (b) T = 653 K and $p_E = 3\times10^5$ Pa, (d) T = 703 K and $p_E = 3\times10^5$ Pa. The ethylbenzene partial pressure was fixed to 35 Pa in each case.

Figure SG2: Simulated and experimental rates per unit mass of catalyst for the alkylation of benzene with ethene. (a) Constant benzene partial pressure of 10×10^5 Pa at 653 K; (b) constant ethene partial pressure of 3×10^5 Pa at 653 K. The ethylbenzene partial pressure was fixed to 35 Pa in each case.

Figure SG3: Simulated and experimental rates per unit mass of catalyst for the alkylation of benzene with ethene. (a) Constant benzene partial pressure of 10×10^5 Pa at 703 K; (b) constant ethene partial pressure of 3×10^5 Pa at 703 K. The ethylbenzene partial pressure was fixed to 35 Pa in each case.

Figure SG1

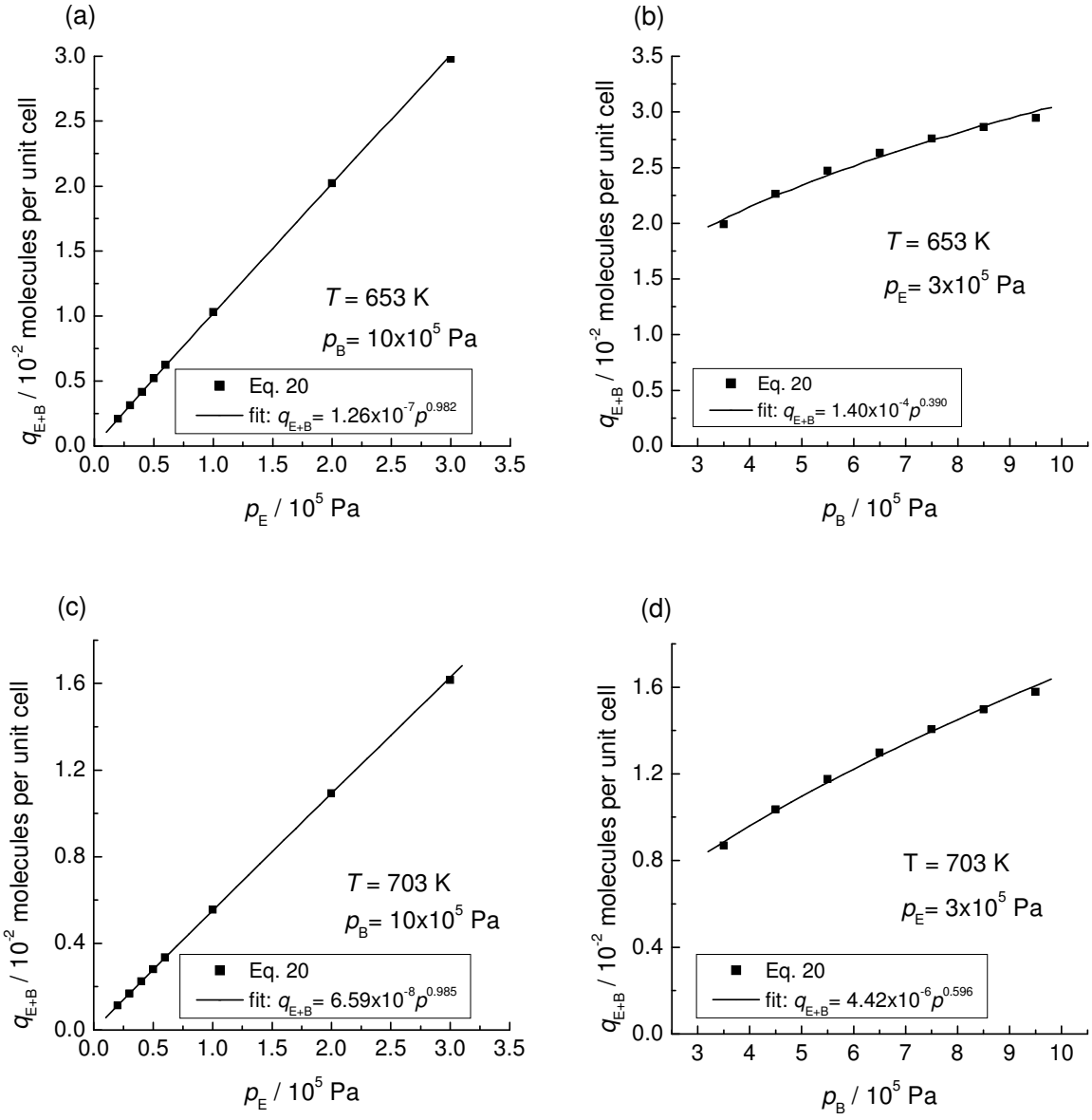
(a)
q_{E+B} / 10^{-2} molecules per unit cell
p_E / 10^5 Pa
T = 653 K
p_B= 10x10^5 Pa
Eq. 20
fit: q_{E+B}= 1.26x10^{-7} $p^{0.982}$
(b)
q_{E+B} / 10^{-2} molecules per unit cell
p_B / 10^5 Pa
T = 653 K
p_E= 3x10^5 Pa
Eq. 20
fit: q_{E+B}= 1.40x10^{-4} $p^{0.390}$
(c)
q_{E+B} / 10^{-2} molecules per unit cell
p_E / 10^5 Pa
T = 703 K
p_B= 10x10^5 Pa
Eq. 20
fit: q_{E+B}= 6.59x10^{-8} $p^{0.985}$
(d)
q_{E+B} / 10^{-2} molecules per unit cell
p_B / 10^5 Pa
T = 703 K
p_E= 3x10^5 Pa
Eq. 20
fit: q_{E+B}= 4.42x10^{-6} $p^{0.596}$

Figure SG2

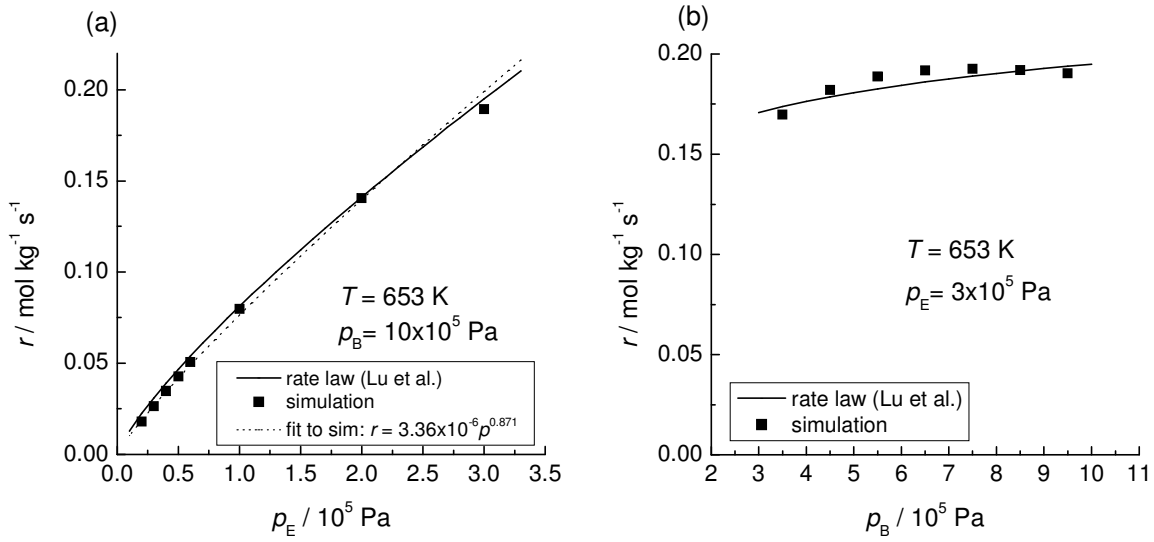

Figure SG3